Chemical Geology 550 (2020) 119628

Contents lists available at ScienceDirect

Chemical Geology

journal homepage: www.elsevier.com/locate/chemgeo

Invited research article

Engineered carbon mineralization in ultramafic rocks for CO_2 removal from air: Review and new insights

Peter B. Kelemen[a,*], Noah McQueen[b], Jennifer Wilcox[b], Phil Renforth[c], Greg Dipple[d], Amelia Paukert Vankeuren[e]

[a] Dept. of Earth & Environmental Sciences, Columbia University, Lamont Doherty Earth Observatory, Palisades, NY, USA
[b] Clean Energy Conversions Lab, Dept. of Chemical Engineering, Worcester Polytechnic Institute, Worcester, MA, USA
[c] Research Centre for Carbon Solutions, School of Engineering and Physical Sciences, Heriot-Watt University, Edinburgh, UK
[d] Mineral Deposit Research Unit, Dept. of Earth, Ocean, and Atmospheric Sciences, University of British Columbia, Vancouver, BC, Canada
[e] Geology Dept., California State University, Sacramento, Sacramento, CA, USA

ARTICLE INFO

Editor: Balz Kamber

Keywords:
Carbon mineralization
Mineral carbonation
Enhanced weathering
Mine tailings
Magnesite
Caustic magnesia
Peridotite
Serpentinite
Ultramafic rocks

ABSTRACT

Carbon Dioxide removal from air (CDR) combined with permanent solid storage can be accomplished via carbon mineralization in ultramafic rocks in at least four ways:

1. *Surficial* CDR: CO_2-bearing air and surface waters are reacted with crushed and or ground mine tailings, alkaline industrial wastes, or sedimentary formations rich in reactive rock fragments, all with a high proportion of reactive surface area. This can be implemented at a low cost, but most proposed methods have a very large area footprint at the gigatonne scale. The area requirement can be greatly reduced by calcining (heating to produce pure CO_2 for permanent storage or use) followed by recycling of MgO, CaO, Na_2O, … Such looping methods have predicted costs that are as low or lower than for direct air capture with synthetic sorbents or solvents (DACSS), and a similar area footprint.

2. In situ CDR: CO_2-bearing surface waters are circulated through rock formations at depth. These methods potentially have a cost similar to that of surficial carbon mineralization, and a giant storage capacity with reduced surface area requirements, but they involve uncertain feedbacks between permeability, reactive surface area, and reaction rate, providing a fascinating topic for fundamental research. Furthermore, the size, injectivity, permeability, geomechanics, and microstructure of key subsurface reservoirs for in situ CDR remain almost entirely unexplored.

3&4. Combined partial enrichment of CO_2 using direct air capture with synthetic sorbents (DACSS) plus *surficial* carbon mineralization (3) or in situ carbon mineralization (4). Energy requirements and total costs for partial enrichment of CO_2 are substantially lower than for enrichment to high purity. CO_2 enriched air can be sparged through mine tailings at the surface, and/or through water to increase dissolved carbon concentrations prior to circulation through rock reactants. Such combined or hybrid approaches have not been investigated thoroughly, and offer many avenues for optimization.

1. Introduction

Recently, the Intergovernmental Panel on Climate Change (IPCC) and other authoritative sources have concluded that annual removal of more than ten gigatons (Gt) CO_2 from air (CDR, aka "negative emissions") will be required by mid-century to keep global warming below 1.5 to 2 °C (e.g., IPCC, 2014; IPCC, 2018; UNEP, 2018). The National Academies of Sciences, Engineering & Medicine (2019, NA19) reviewed negative emissions technologies, and proposed a US research agenda to move them forward. One such technology is carbon mineralization, in which CO_2 in air and water react with Mg- and Ca-rich rocks (ultramafic rocks) and industrial wastes of similar composition to form solid carbonate minerals. This is a relatively untested but potentially inexpensive and practical way to achieve CDR at a scale of 1 to 10 Gt/yr, as quantified throughout the following five sections of this paper.

Engineered carbon mineralization is better known as a potential technology for storing CO_2 captured elsewhere. Storing CO_2 via reaction with common rocks and minerals has been considered for 30 years (Lackner et al., 1995; Seifritz, 1990). More recently, the possibility of carbon mineralization using alkaline industrial waste products such as

* Corresponding author.
E-mail address: peterk@LDEO.columbia.edu (P.B. Kelemen).

https://doi.org/10.1016/j.chemgeo.2020.119628
Received 17 September 2019; Received in revised form 1 April 2020; Accepted 11 April 2020
Available online 06 May 2020

steel slag and demolition waste has been added to the palette of options (e.g., Gadikota et al., 2015; Huijgen et al., 2007; Pan et al., 2012; Renforth, 2019; Renforth et al., 2009; Renforth et al., 2011; Sanna et al., 2014). Mineralization occurs naturally during weathering of Mg- and/or Ca- rich, Al-poor materials (e.g., "ultramafic rocks" composed mainly of the minerals olivine, serpentine, brucite, and/or wollastonite, and/or industrial wastes with similar, ultramafic compositions). In this paper, we focus on the possibility that engineered carbon mineralization could remove significant quantities of CO_2 from air.

This paper reviews carbon mineralization kinetics and the major pathways for CO_2 removal from air (CDR), combined with solid storage, via carbon mineralization, including estimates of rates, capacities and cost. The paper arises from our contributions to Chapter 6 of NA19. Unlike that Chapter, and Kelemen et al. (2019a), this paper does not review methods that use carbon mineralization to store CO_2 captured elsewhere, and instead focuses on CDR plus solid storage. Many sections in this paper that are similar to NA19 Chapter 6 are abridged here. This paper updates figures and calculations, and includes authors who contributed significantly to NA19 but were not on the National Academy committee.

Somewhat to our surprise, in the course of preparing this paper, we have added several significant, new, potentially transformative ideas, including data and estimates on the energy cost and CO_2 emissions arising from grinding solid reagents (Section 2, Figs. 3 to 5 and associated text), recycling of carbonated mine tailings to capture additional CO_2 in each cycle (Section 4, Fig. 7 and associated text) and hybrid methods combining partial enrichment of CO_2 in air via direct air capture with synthetic sorbents or solvents (DACSS) with either surficial or in situ carbon mineralization (Section 6, Figs. 11, 12 and associated text). Though they are less than a year old, in hindsight some of these ideas now seem quite obvious. This emphasizes the ongoing potential for significant breakthroughs arising from research on this relatively young and unexplored technology.

The methods reviewed here emulate and accelerate spontaneous, natural processes, making use of the abundant chemical potential energy that is available where rocks from the Earth's deep interior are emplaced at and near the surface, where they are far from equilibrium with the atmosphere and hydrosphere. Because they utilize this naturally available chemical energy, these methods offer low cost routes to CDR and permanent storage in inert, solid, non-toxic minerals. New and revised cost estimates in this paper indicate that engineered carbon mineralization, and hybrid methods involving direct air capture with synthetic sorbents or solvents (DACSS) plus mineralization, are likely to be less expensive methods for CDR, per ton of CO_2, compared to direct air capture alone.

2. Reactions and rates

Mg-rich, Ca-bearing, highly reactive rocks include mantle peridotite and ultramafic intrusions. These provide a key source of alkalinity for Mt to Gt storage of CO_2 via carbon mineralization. Prior to alteration during reaction with fluids, these rocks are rich in the minerals olivine and pyroxene. In altered ultramafic rocks, the mineral brucite (0 to 10% of altered peridotite by weight), together with some fibrous polytypes of serpentine (often, chrysotile), provide the best reactants for rapid CDR at surface conditions, for example in mine tailings.

The mineral wollastonite ($CaSiO_3$) reacts more rapidly than olivine and pyroxene. However, wollastonite occurs in small bodies and limited amounts. Estimated global reserves of wollastonite are ~100 M tons (Curry, 2020), whereas there are tens to hundreds of trillions of tons of peridotite within 3 km of the Earth's surface (e.g., Kelemen et al., 2011). The Ca-bearing component in many alkaline industrial wastes is similar in composition to wollastonite, but is less fully crystalline and thus potentially faster to dissolve and react. However, relatively low Ca and Mg concentrations in some industrial wastes limit the CO_2 storage capacity per ton of solid reactant (NA19 Table 6.1). Nevertheless, these materials may offer a means to remove more than one Gt CO_2 from the atmosphere per year if greenhouse gas emissions from these industries were decreased together with mineralization in wastes and by-products (Renforth, 2019).

Rocks including abundant plagioclase feldspar (basalts, gabbros) react more slowly than peridotite (e.g, NA19, Gadikota et al., 2020, Kelemen et al., 2011), and undergo less extensive carbon mineralization during natural, low temperature alteration and weathering, so that we do not consider them to be ideal for CDR, except perhaps as an additive to agricultural soils for enhanced weathering (Beerling et al., 2018). Thus, in this paper we focus on mantle peridotite and ultramafic intrusions. However, where basaltic lava formations contain horizons rich in amorphous glass, these react more rapidly than olivine (experimental data in Gislason and Oelkers, 2003, comparisons in Kelemen et al., 2011 and NA19), and provide targets for CDR. Though we do not focus on this opportunity in this paper, we wish to emphasize that it seems wise to explore for areas where abundant basaltic glass might facilitate CDR.

In carbon mineralization, CO_2 reacts with minerals rich in Ca and Mg to form carbonates, such as calcite ($CaCO_3$), magnesite ($MgCO_3$), and dolomite ($CaMg(CO_3)_2$, and a host of metastable, hydrated carbonate minerals: hydromagnesite ($Mg_5(CO_3)_4(OH)_2{\cdot}4H_2O$), nesquehonite ($Mg(HCO_3)(OH){\cdot}2(H_2O)$), dypingite ($Mg_5(CO_3)_4(OH)_2{\cdot}5H_2O$), hydrotalcite ($Mg_6Al_2CO_3(OH)_{16}{\cdot}4H_2O$), and so on. Reaction of olivine and pyroxene with aqueous fluids at upper crustal pressures and temperatures less than ~300 °C converts silicate minerals to brucite ($Mg(OH)_2$), serpentine ($Mg_3Si_2O_5(OH)_4$), talc ($Mg_3Si_4O_{12}(OH)_2$), and various other hydrous phases. In rocks with Mg/Si > 1.5, excess Mg forms brucite ($Mg(OH)_2$). In turn, hydrous silicates and brucite can also react with CO_2 to form carbonates.

Some idealized reactions are as follows:

$$\text{wollastonite } CaSiO_3 + CO_2 \leftrightarrow CaCO_3, \tag{1}$$

$$\text{olivine } Mg_2SiO_4 + 2CO_2 \leftrightarrow 2MgCO_3 + SiO_2, \tag{2}$$

$$\text{pyroxenes } CaMgSi_2O_6 + 2CO_2 \leftrightarrow CaMg(CO_3)_2 + 2SiO_2, \tag{3}$$

$$\text{serpentine polytypes } Mg_3Si_2O_5(OH)_4 + 3CO_2 \leftrightarrow 3MgCO_3 + 2SiO_2 + 2H_2O, \tag{4}$$

$$\text{and brucite } Mg(OH)_2 + CO_2 \leftrightarrow MgCO_3 + H_2O \tag{5}$$

Wollastonite, olivine, and brucite react relatively rapidly, as do fibrous serpentines with high surface area to volume ratios, such as asbestiform chrysotile. Ca and Mg in alkaline industrial wastes react at about the same rate as wollastonite, especially when they are not incorporated in alumino-silicate compounds. A more extensive discussion of kinetic data for carbon mineralization is given in NA19, Chapter 6.

These reactions are spontaneous and exothermic; carbonate minerals are the "ground state" for CO_2 in near-surface rock systems such as Mg-Ca-C-O-H and Mg-Ca-Si-C-O-H (Fig. 1). The energy density of unreacted olivine in the presence of H_2O or CO_2 at low temperature is ~2 GJ/m^3, only ~20 times smaller than the energy density of gasoline. A key goal of research on engineered carbon mineralization is to use this naturally available reservoir of chemical potential energy to reduce external energy inputs and costs for CDR.

Reaction times for different minerals and grain sizes, approximated using data on mineral dissolution rates, are illustrated in Fig. 2 (reproduced from NA19, Fig. 6.6).

$$X(t) = \frac{D_0^3 - (D_0 - 2W_r V_m t)^3}{D_0^3} \tag{6}$$

where V_m is the molar volume of the material (m^3 mol^{-1} assumed here to be 40 cm^3 mol^{-1}, although the molar volume of natural primary silicate minerals ranges from this up to >100 cm^3 mol^{-1}), and t is the dissolution time (s). Grinding produces a particle size range, P(D). Here

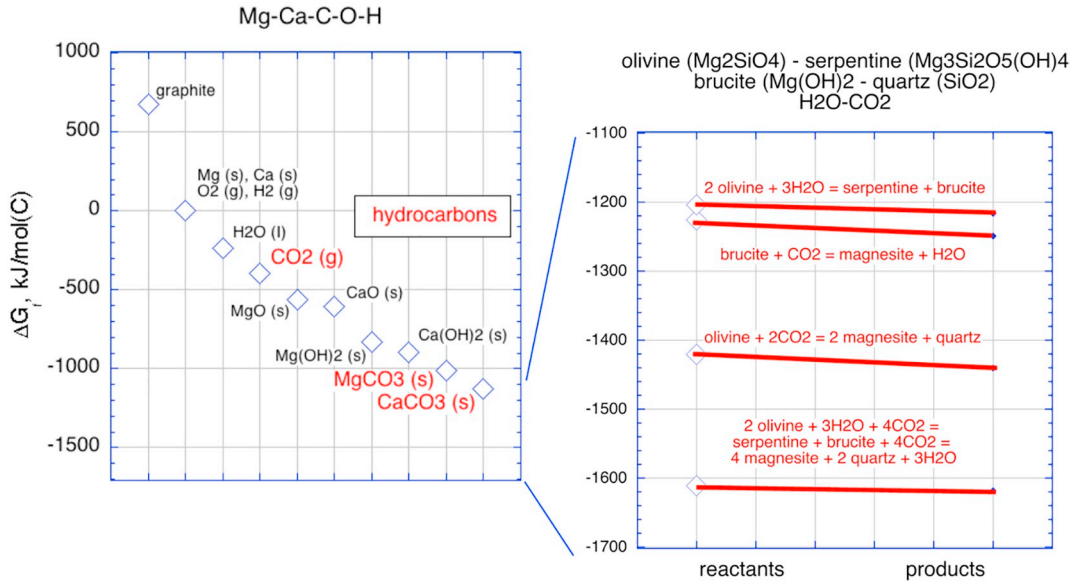

Fig. 1. Standard state Gibbs free energies of formation and reaction for selected compounds in the chemical systems Mg-Ca-C-O-H and Mg-Ca-Si-C-O-H. Values for solid phases are for metals (Mg, Ca) and crystalline minerals graphite (C), periclase (MgO), lime (CaO), brucite ($Mg(OH)_2$), portlandite ($Ca(OH)_2$), magnesite ($MgCO_3$), and calcite ($CaCO_3$), plus minerals in the righthand panel as labeled. The rectangle labeled "hydrocarbons" encompasses the range of Gibbs free energies of formation for common hydrocarbon species (e.g., methane, ethane, and butane) per mole of carbon. Figure reproduced from NA19, Chapter 6, Fig. 6.1).

we use a gamma distribution $\Gamma(\alpha)$ previously coupled to a shrinking core model (Gbor and Jia, 2004)

$$\mathrm{P}D = D\alpha - 1e - D\beta\beta\alpha\Gamma(\alpha) \quad (7)$$

where α and β are empirically-derived coefficients that describe the variability of particle diameter (D):

$$\mathrm{P}(D) = \frac{D^{\alpha-1}e^{-D/\beta}}{\beta^{\alpha}\Gamma(\alpha)} \quad (8)$$

A maximum mean particle size was simulated with a typical particle size distribution from comminution to achieve 90% dissolution. Dissolution rate ranges are shown for brucite ($Mg(OH)_2$), chrysotile serpentine ($Mg_3Si_2O_5(OH)_4$), minerals in the plagioclase feldspar solid solution [Na endmember albite (Ab - $NaAlSi_3O_8$), Ca endmember anorthite (An - $CaAl_2Si_2O_8$), oligoclase (Olg – 10-30% An), andesine (30–50% An), labradorite (Lab – 50-70% An), bytownite (Byt – 70-90% An)], wollastonite ($CaSiO_3$), and Mg-rich olivine (Mg_2SiO_4), derived using rate data from Palandri and Kharaka, 2004 for all minerals except chrysotile serpentine (Thom et al., 2013), assuming pH from 3 to 7, 25 °C (blue bars) and 180 °C (orange bars), and negligible effects of mineral solution saturation. Rates determined from mineral dissolution experiments are shown for (a) basalt added to artificial soil at ~10 °C (Manning et al., 2013), (b) basalt/dunite/hazburgite added to seawater at 25 °C (Rigopoulos et al., 2018b), (c) Mg-rich olivine added to soil at 25 °C (ten Berge et al., 2012), (d) Mg-rich olivine added to seawater at 25 °C (Montserrat et al., 2017), and (e) Mg-rich olivine added to soil at 19 °C, (Renforth et al., 2015).

To illustrate the relationships between rates, grain size, surface energy, grinding energy, and CO_2 emissions, we have added Figs. 3, 4 and 5. Most comminution technology is inefficient, and the efficiency declines with increasing surface area (Fig. 3). According to Tromans (2008) between 5 and 10% efficiency may be possible given energy dissipation from strain during crushing. Using current methods, it is possible to create surface areas of 1–10 m^2/g using 10–100 kWh/t. However, if efficiencies were improved, it could be possible to reach 10–100 m^2/g at ~100–500 kWh/t. In turn, such relatively minor changes in grinding cost would have a dramatic effect on the rate of carbon mineralization. Fig. 3 also illustrates that at the current emissions intensity of electricity (for example, ~400 gCO_2/kWh in the UK), using 100 kWh to attain a grain size of 10 m^2/g in a ton of rock would release 40 kg CO_2, which would reduce the net carbon uptake via mineralization of typical ultramafic rock by a few percent. Future use of low carbon electricity could reduce the emissions intensity to ~50 g CO_2/kWh, so that CO_2 emissions during grinding would be negligible.

Fig. 4 supplements Fig. 2, using grinding energy estimated from the data in Fig. 3 to illustrate the energy required to achieve a given grain size, and thus a given time for carbon mineralization using different materials. For reference, 100 MJ/ton corresponds to ~28 kWh, and a cost of $1.40 to $4.20 per ton of rock at electricity costs of $0.05 to $0.15/kWh.

Fig. 5 emphasizes that the shrinking sphere approximation used to construct Figs. 2 and 4 may overestimate the energy requirements for grinding by an order of magnitude in some parameter ranges, still further reducing the importance of the energy cost of grinding when computing the overall cost and emissions consequences of proposed carbon mineralization methods.

3. Surficial CDR

3.1. One-time, one-year CDR using mine tailings

Mine tailings and some alkaline industrial wastes provide "low-hanging fruit" as rock reactants for CO_2 removal from air (CDR) and storage via carbon mineralization. Tailings and some wastes have high surface area to volume ratios compared to subsurface geological formations, and are currently produced for other reasons, thus providing nearly "cost-free" feedstock for CDR. Ultramafic intrusions, with Mg to Si ratios approaching 2 and abundant olivine, are mined for platinum-group elements, Cr, and diamonds. Ultramafic lava flows (komatiites) and tectonically exposed and weathered mantle peridotites are an important source of Ni and Cr. Mafic intrusions approximately comparable in composition to basaltic lavas are mined for platinum group elements, Ni and Cr. Smelting of these ores produces ultramafic and mafic glass, which probably reacts faster than compositionally identical minerals at the same grain size. Alkaline industrial wastes are varied, and it is beyond the scope of this paper to review their compositions. However, as an example, slag derived from smelting iron ore includes abundant Ca-Al silicate, formed by Ca derived from limestone together with Al

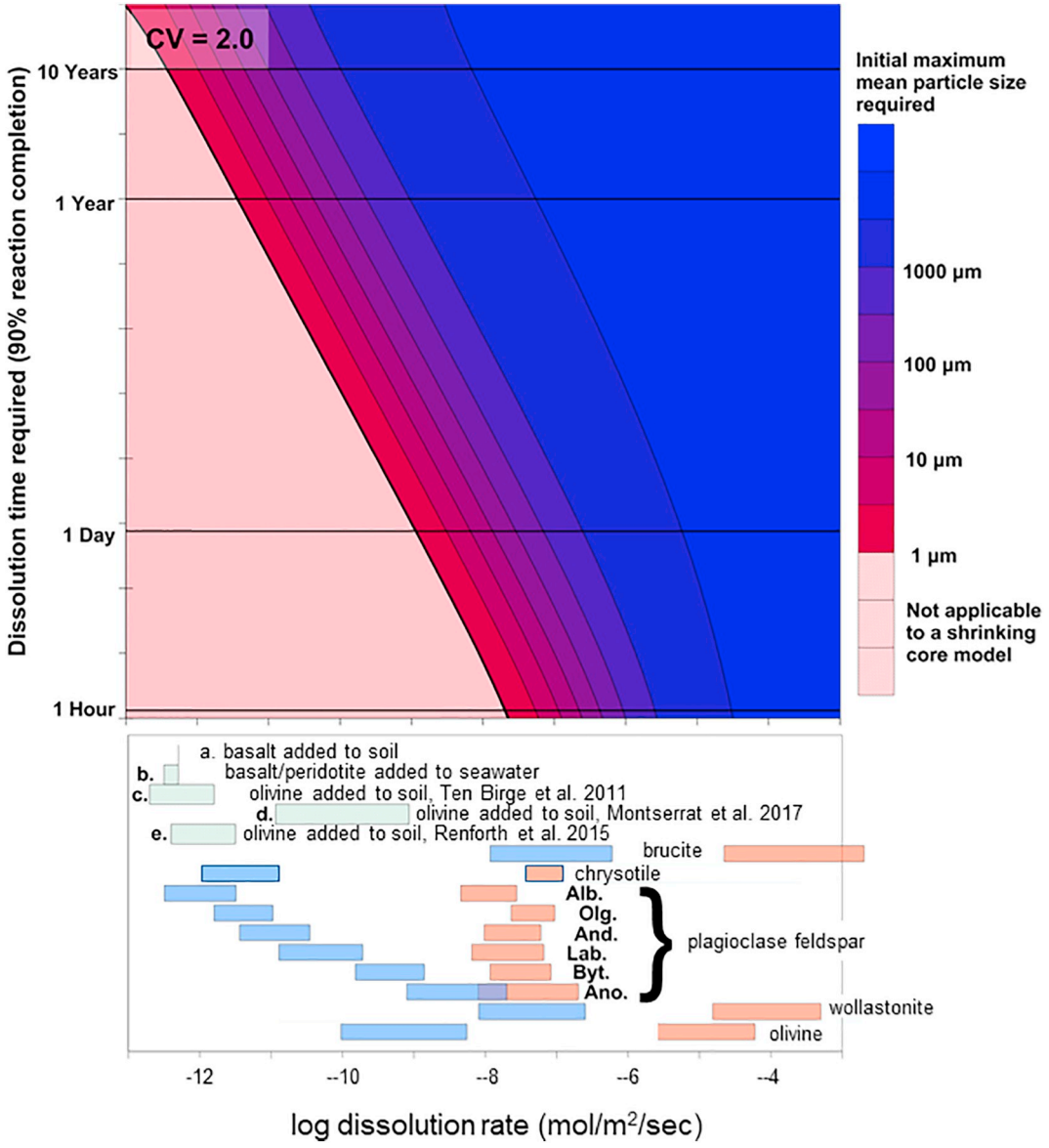

Fig. 2. Figure reproduced from NA19, Fig. 6.6. Relationship between initial mean particle size in a typical particle size distribution (covariance σ/μ, CV = 2.0), mineral dissolution rate, and time required to achieve 90% by volume dissolution of an arbitrary mineral using a shrinking core model. For a given extent of dissolution (*X*), the initial particle diameter (D_0; m) can be related to dissolution rate (W_r; mol m^{-2} s^{-1}) through a shrinking core model.

and Si extracted from the iron ore.

The CO_2 uptake and storage capacity for complete carbonation in these materials is significant: 0.62 tons of CO_2 per ton of olivine reactant, 0.76 tons of CO_2 per ton of brucite reactant, and ~0.4 to 0.5 tons of CO_2 per ton of pyroxene, serpentine, wollastonite, and industrial waste similar to wollastonite in composition. Based on our informal assessment of the volume of existing mines, we estimate that the total mass of existing ultramafic tailings is <10 billion tons, of which an unknown proportion has already been carbonated during natural weathering. Annual production of new ultramafic mine tailings is about 420 million tons (Power et al., 2013b). Dipple and co-workers (Harrison et al., 2012; Power et al., 2011; Wilson et al., 2014) emphasize that at surface conditions (~10–30 °C, $P(CO_2)$ ~0.004 atm) most minerals in ultramafic and mafic rocks are relatively slow to react, with the exception of brucite and some fibrous serpentine. Thus, they focus on rapid carbonation of "*labile Mg*" contained in the latter two materials. Typically, labile Mg comprises ~3 wt% of partially to fully serpentinized, ultramafic mine tailings, with a practical maximum of ~10 wt % Mg in most settings (Vanderzee et al., 2019). Carbonation of this Mg (~24 g/mol) in 420 Mt of newly produced mine tailings would consume <75 million tons of CO_2 per year. If production of ultramafic tailings increases from 420 Mt to 1–3 Gt/yr by 2100 (Renforth, 2019), then this upper bound for annual CO_2 uptake in tailings would also increase by a factor of five to fifteen.

Because the annual storage capacity of newly mined ultramafic tailings is small compared to human emissions, the question arises whether one could mine ultramafic rock for the purpose of creating fine-grained rock reactants for CDR. Quarrying, crushing, and grinding of mine tailings costs ~$10 per ton (Infomine, 2018). Carbonating 1 to 10 wt% labile Mg (2 to 16 wt% MgO), consuming ~2 to 18 wt% CO_2 in one year, would correspond to $500 to $55 per ton of CO_2. This cost is comparable to estimates for direct air capture with synthetic sorbents (DACSS) plus subsequent storage in deep sedimentary formations, within the uncertainties of all values. Additional costs per ton to speed carbon mineralization and/or reduce the area requirements for surficial CDR (e.g., spreading tailings in thin sheets, stirring them, providing access to air flow) can be negligible. For example, reprocessing diamond mine tailings, including excavation, transport and extraction of

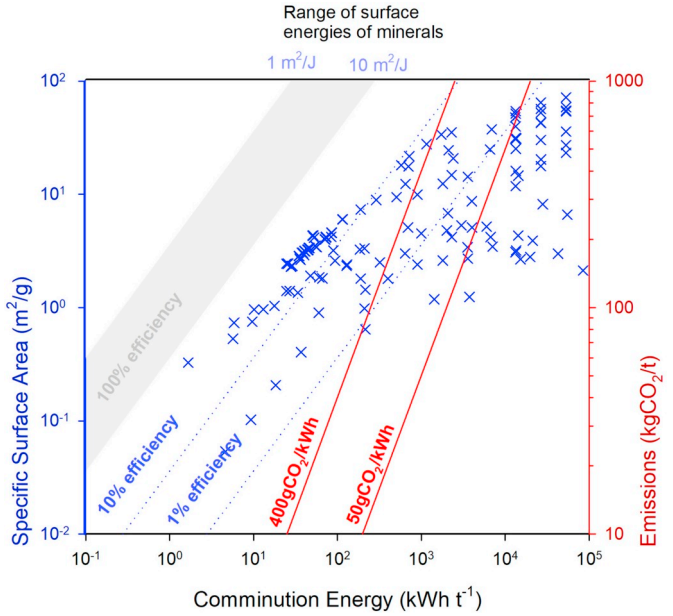

Fig. 3. Relationship between comminution energy and specific surface area (blue) and comminution energy and CO_2 emissions (red). Blue crosses are empirical data on BET derived surface area values for a range of minerals that have undergone comminution (Atashin et al., 2015, Baláž et al., 2008, Choi et al., 2009, Haug et al., 2010, Kleiv and Thornhill, 2006, Li and Hitch, 2017, Mortsell and Svensson, 1951, Rigopoulos et al., 2018a, Rigopoulos et al., 2018b, Stamboliadis et al., 2009, Wang et al., 2004). Most common minerals have surface energies between 1 and 10 m^2/J (grey shaded area on the diagram, Tromans, 2008) which is a thermodynamic lower limit for comminution energy. Compared to this limit, most comminution technologies are <1% efficient at creating new surface area. (For interpretation of the references to colour in this figure legend, the reader is referred to the web version of this article.)

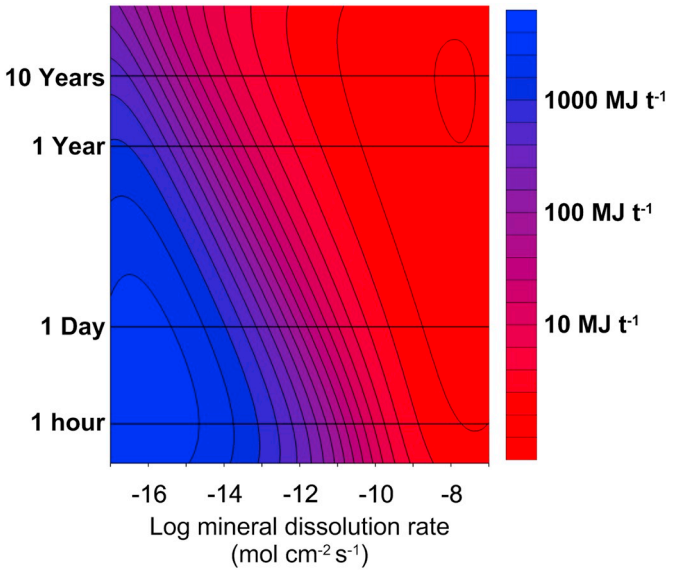

Fig. 4. The relationship between electricity requirements (colour scale), mineral surface area normalised dissolution rate (horizontal axis), and time to reach 90% completion (vertical axis) in the shrinking core model, using Hukki's empirically validated general relationship between initial mean particle size and comminution energy requirements (see Martins, 2016).

diamonds, costs less than $2/ton of tailings (anonymous personal communication, 2018) and soil can be excavated for $1 to $2/ton (Caterpillar, 2018).

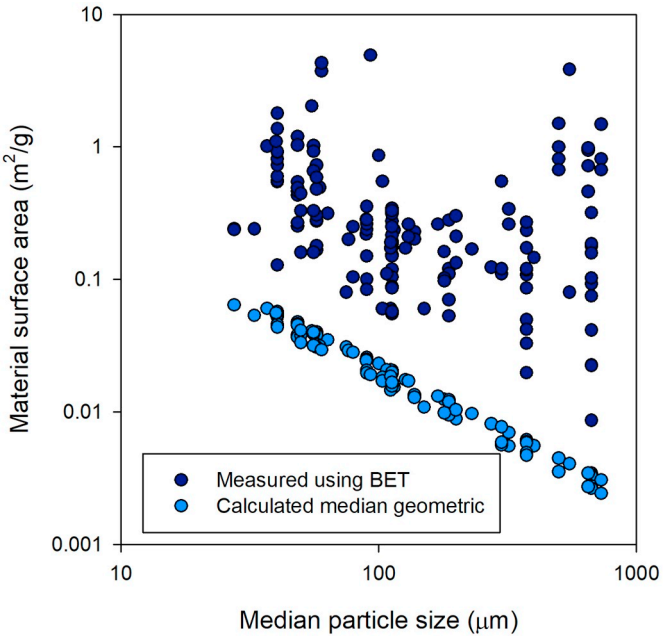

Fig. 5. Data (Brantley and Chen, 1995; Brantley and Mellott, 2000, and references therein) on calculated spherical geometric and BET surface area (BET: Brunauer-Emmett-Teller surface area, Brunauer et al., 1938). Brantley and Mellott, 2000 primarily present data for plagioclase feldspars, whereas Brantley and Chen, 1995 provide data for pyroxene and amphibole minerals. The range of values is often attributed to internal micro-porosity created as either a consequence of mineral alteration during weathering or as a consequence of comminution.

Creating tailings to consume 1 to 10 wt% labile Mg for CDR in one year might produce 10 to 100 Gt of tailings (5 to 50 km^3, with a density of 2 tons/km^3) per Gt of CO_2 removed from air. This corresponds to a layer 10 to 90 μm thick over the entire 510 million km^2 area of the oceans, 0.4 to 3 mm thick over the entire 14 million km^2 of arable land worldwide, or 30 to 260 m thick over Washington, D.C. (177 km^2), per Gt of CO_2 captured from air and stored. Of course, practical application of such methodologies on land would not involve any of those scenarios, and instead almost certainly would entail spreading layers centimeters thick on marginal lands (~27 million km^2, FAO, 2011). Thus, for example, if the layer were 10 cm thick, the area requirement would be about 50,000 to 500,000 km^2 per Gt of CO_2 removed from air. Similarly, Wilson et al. (2014) demonstrated that komatiite tailings weather naturally at a rate that captures 2.5 kg CO_2 from air per m^2 of tailings land surface per year. For this process to capture 1 Gt CO_2 per year, tailings would have to be spread over about 400,000 km^2. Depending on scale, location and societal preferences, transporting and storing or disposing of such large volumes of tailings could be difficult to implement, except in a dire climate emergency. Furthermore, ultramafic tailings commonly contain high concentrations of Ni, Cr and other trace metals which – if introduced into food or water – could be harmful to human health. This is uncertain, as discussed at more length in Section 3.4.

Several ways to reduce the area footprint and environmental impact of surficial carbon mineralization suggest themselves, one involving multi-year weathering of tailings, as previously described in NA19 and updated here, and another reported for the first time in this and a companion paper, involving repeated calcining and weathering of $MgCO_3$-MgO, together with permanent storage or use of produced CO_2, and a third, dispersing small amounts of tailings over large areas of agricultural land. These are outlined in the next three sub-sections of the paper.

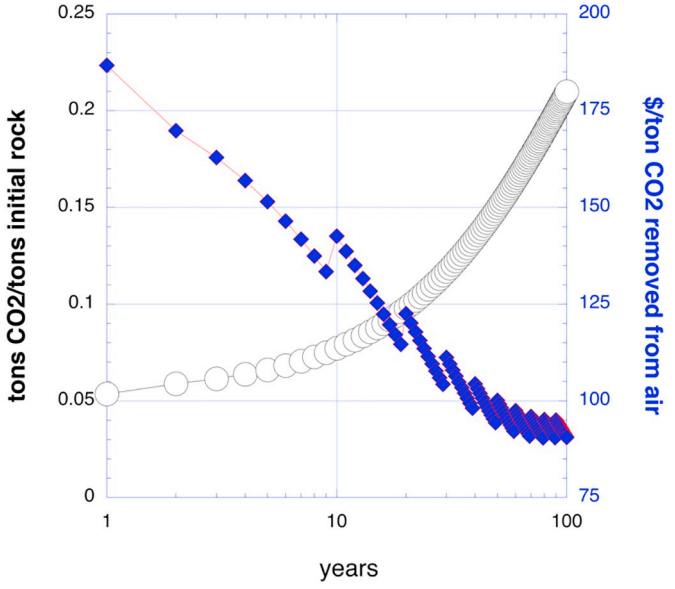

Fig. 6. Weight fraction CO_2 removed from air and stored in ultramafic mine tailings with 3 wt% labile Mg, as a function of time. The initial rock reactant contains 7.2 wt% brucite, 40 wt% olivine and 52.8 wt% serpentine, with constant reaction rates (mass fraction per second) of $3\ 10^{-8}$, $3\ 10^{-10}$, and $3\ 10^{-12}$, respectively. Cost based on $10/ton to mine and grind rock, and $1/ton every 10 years to stir tailings.

3.2. Extended weathering of mine tailings

In addition to rapid carbonation of labile Mg, some olivine and a small amount of non-fibrous serpentine in ultramafic tailings will also undergo carbonation over decades of weathering. To calculate how much, we use kinetic data in NA19, the assumption of constant reaction rates (e.g., NA19, Fig. 6.3), a conversion rate for brucite in typical mine tailings of $3\ 10^{-8}$/s (mass fraction per second, via first-order kinetics), and conservative olivine and non-fibrous serpentine conversion 10^2 and 10^4 times smaller than brucite, respectively, together with a cost of $10/ton to produce tailings, and $1/ton to stir them every ten years. This calculation yields the estimate that carbon mineralization of typical mine tailings with 3 wt% labile Mg (7.2 wt% brucite, 40 wt% olivine, 52.8 wt% serpentine) could capture and store about 21 wt% CO_2 in 100 years (Fig. 6). This would cost approximately $90 per ton of CO_2 – comparable to the lowest estimated costs of DAC systems – and produce about 2 km^3 of tailings per Gt of CO_2 captured and stored (a 10 m layer over Washington, D.C., or – more seriously – a 10 cm layer over 20,000 km^2 rather than ~150,000 km^2 for the one-time, one-year scenario with 3% labile MgO in the previous section). However, extensive areas of thinly layered tailings would have to be maintained for many decades, potentially rendering implementation at a scale of tens of Gt over decades impractical. It might be possible to reach a similar goal by dispersing ultramafic tailings on coastlines or the shallow seafloor (Hartmann et al., 2013; Köhler et al., 2013; Köhler et al., 2010; Montserrat et al., 2017; Rigopoulos et al., 2018b; Schuiling and Krijgsman, 2006), but environmental impacts and barriers to social acceptance are uncertain, while monitoring and verification would be difficult, as discussed further in sub-section 3.4.

3.3. Repeated weathering and calcining of MgO-$MgCO_3$

Another way to reduce the cumulative volume of tailings required for CDR at >1 Gt/yr would be to "*calcine*" and re-use tailings over and over again. Here we provide an overview this idea, which is developed more fully in a separate paper (McQueen et al., 2020) and in a Patent Application 62/865,708, "Systems and Methods for Enhanced Weathering and Calcining for CO_2 Removal from Air," filed on June 24, 2019. Magnesite undergoes thermal decarbonation (*calcining*) to form "*caustic MgO*" (amorphous or poorly crystalline MgO) + CO_2 at 500–900 °C (Mitina et al., 2015). This temperature is lower than for calcining of calcite and dolomite, reducing the energy required for heating. Caustic MgO produced by calcining has a small grain size and high surface area to volume ratio, which aids in later carbonation steps (Ebrahimi-Nasrabadi et al., 2013). Caustic MgO would be spread in a thin layer. Weathering of MgO will remove CO_2 from air to form more $MgCO_3$ and or hydrous Mg-carbonate minerals such as nesquehonite and hydromagnesite. CO_2 produced by calcining would be transported a short distance for permanent geological storage (as reviewed in NA19, Chapter 7, and Kelemen et al., 2019a), or sold for use (as an additive to building materials, for enhanced oil recovery, or for synthesis of hydrocarbons).

Geological magnesite deposits can be mined for this purpose, and this would probably be the least expensive approach. Worldwide magnesite reserves are ~8.5 Gt (Bray, 2020), containing ~4.4 Gt CO_2. Little of this is mined annually at present (~30 Mt per year). Large magnesite deposits are stratiform, chemical sediments, and/or chemically deposited concretions within sediments (Alçiçek, 2009; Fallick et al., 1991; Pohl, 1990; Zedef et al., 2000), which are relatively inexpensive to quarry and grind via surface mining. If ¼ of global magnesite reserves were mined and used for repeated cycles of CDR, extraction of CO_2, and re-use of MgO, this could provide a sink for ~1 Gt CO_2 per cycle.

The area requirement for this process depends on optimizing the thickness of MgO layers to be exposed for weathering, and the rate of CO_2 capture in specific climates, both of which are poorly known. However, here we provide an illustrative set of estimates. It is likely that caustic MgO produced by calcining of magnesite, reacts with atmospheric CO_2 + H_2O to form magnesite and/or hydrous Mg-carbonate minerals under conditions of surficial weathering as rapidly as brucite ($Mg(OH)_2$) does. Using the rate of carbonation of brucite in typical mine tailings, ~$3\ 10^{-8}$/s (mass fraction per second, Harrison et al., 2012; NA19, Fig. 6.4, and references therein), yields roughly 100% conversion per year. Capture of 1 Gt CO_2/yr using a 10 cm thick layer of MgO powder, with a density of 2 tons/m^3, would require an area of 4500 km^2. Using slightly different values, McQueen et al. (2020) derive an area requirement of 6100 km^2. To this can be added the footprint of power generation facilities required for calcination and other processes. Following protocols in NA19, Chapter 5, McQueen et al. (2020) estimate that natural gas combined cycle generation is used for electricity generation, this adds 15 km^2, for a total of ~6100 km^2. If instead solar energy is used for all processes, this requires an additional 1400 km^2, for a total of ~7500 km^2.

These area requirements are, of course, much larger than Washington DC. The requirement of ~6100 km^2, using natural gas power generation, is eight times greater than the area of the King Fahd International Airport in Saudi Arabia (776 km^2, Wikipedia, 2019), about half the size of the Nevada Test Site and the surrounding Nevada Test & Training Range in the United States (15,000 km^2, Wikipedia, 2019) and similar to the estimated 7000 km^2 required for removal of 1 Gt CO_2 from air using direct air capture with synthetic sorbents (NA19, Chapter 5).[1] As additional points of comparison, for countries with large magnesite reserves and production, 6100 km^2 is 5.1% of the area of North Korea (2.3 Gt magnesite reserves), 0.2% of Saudia Arabia (significant magnesite production), 0.07% of China (1 Gt), and 0.04% of Russia (2.3 Gt). Faster rates, and correspondingly smaller area requirements, might be expected if the grain size of caustic MgO from calcining is substantially less than the grain size in typical mine tailings,

[1] "The land area requirement … using direct air capture is 7 km^2 per Mt CO_2 if powered by natural gas … Additional land [is] required if … renewable energy (e.g., PV solar panels or concentrated solar thermal) is used."

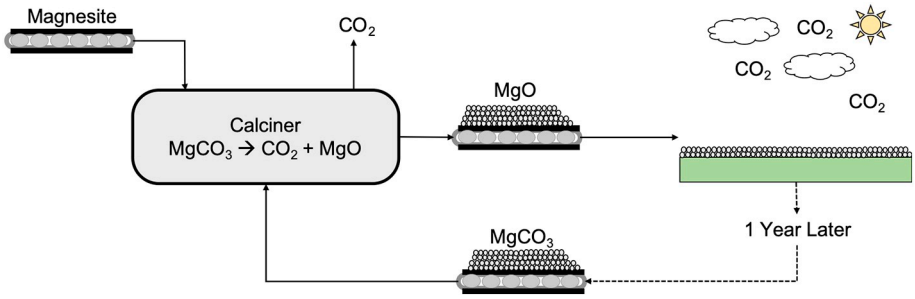

Fig. 7. Schematic illustration of proposed magnesite – MgO + CO_2 cycling method (McQueen et al., 2020).

and/or if the rate of MgO carbonation during weathering, per unit surface area, is significantly faster than experimentally measured for brucite so far. If thicker layers of MgO can be used in the weathering step, this would also reduce the area requirements.

If the entire global magnesite reserve were mined and used for CDR, this could remove about 4 Gt of CO_2 from air per year, for perhaps 10 to 20 years. If caustic MgO produced by calcining cannot be recycled indefinitely, then to continue this procedure at the Gt-scale for additional decades would require use of other materials as feedstock. Similarly, from the outset, additional feedstock would be required to remove >4 Gt/yr. Though it is highly soluble in water, and thus probably not effective except in arid climates, the estimated reserves of Na_2CO_3 are about 25 billion tons (Bolen, 2020), of which about 60 wt% is Na_2O. If all of this were used for CO_2 removal from air, that would yield almost 10 billion tons of CO_2 per year. Limestone (composed mainly of calcite ($CaCO_3$) and dolomite ($CaMg(CO_3)_2$) constitute almost unlimited resources, but require relatively high calcining temperatures. Some alkaline industrial wastes may provide MgO, CaO and/or Na_2O for repeated, enhanced weathering methods. Further analysis will be required to estimate the costs for using these materials.

Tailings from ultramafic rocks provide another alternative. As described above, a first stage of weathering would consume brucite and fibrous serpentine (labile Mg) plus CO_2 to form a limited amount of magnesite. In addition, the first calcining step would modify serpentine via "dehydroxylation", creating a material that combines rapidly with CO_2 to form magnesite, as documented in a large number of studies (Balucan and Dlugogorski, 2013; Balucan et al., 2011; Dlugogorski and Balucan, 2014; Fedoročková et al., 2012; Ghoorah et al., 2014; Larachi et al., 2010; Larachi et al., 2012; Li et al., 2009; Maroto-Valer et al., 2005; McKelvy et al., 2004; O'Connor et al., 2005; Sanna et al., 2014). After a few calcining steps, the recycled solid feedstock would be composed mainly of caustic MgO plus inert SiO_2 and iron oxides. We expect that, after several cycles, labile Mg content will approach the total Mg content of anhydrous ultramafic rock, typically 24 to 27 wt% (40 to 45 wt% MgO) and will capture 44 to 50 wt% CO_2 per year. More generally, the US Geological Survey reports, "Resources from which magnesium compounds can be recovered range from large to virtually unlimited and are globally widespread" (Bray, 2020). In summary, from a practical perspective we expect that economic incentives, rather than the availability of feedstock, will limit the scale of CO_2 removal from air via enhanced weathering with recycling of MgO, CaO and/or Na_2O.

At the current utility scale grid electricity cost of $0.06/kWh (US Energy Information Administration, 2020), starting with magnesite feedstock, assuming natural gas combustion in an oxy-fired furnace for calcining, and accounting for CO_2 emissions from mining, tilling and transportation, McQueen et al. (2020) calculate that this process might achieve CDR at $48 to $193/ton CO_2 net removed, and produce a total amount of CO_2 (both removed from air and captured from furnace emissions) at a cost of $24 to $98/ton. Thus, the cost of this method may be comparable to, or less expensive than, optimistic future projections of the cost of CO_2 net removed via DACSS using similar parameters for energy costs, efficiency and so on ($94/ton, Keith et al., 2018, ≥$89/ton, NA19, Table 5.10). For further discussion of estimated costs for MgO-looping, and comparison with proposed methods for DACSS, please see McQueen et al. (2020).

In conclusion, repeated re-use of magnesite or ultramafic rock tailings, to produce CO_2 via calcining and MgO for CDR via weathering, could be cost competitive with DACSS, and has an area requirement similar to DACSS. It will be important to test the efficacy of MgO cycling, particularly the rate of CDR during weathering, and to optimize layer thickness, stirring methods (if any) and area requirements through a large number of relatively simple but somewhat time-consuming tests. Using feedstock rich in Mg, Ca and/or Na, looping technologies could support processes removing many gigatons of CO_2 from air each year for decades to come. That said, since current, global CO_2 utilization consumes <200 Mt/yr (based on ~80 Mt/yr in the US, Wilcox et al., 2020), removing gigatons of CO_2 from the atmosphere would require extensive, reliable, long-term commitments of government support for permanent storage, or a dramatic change in demand for CO_2-based products (e.g., Hepburn et al., 2019).

3.4. Diffuse dispersal of Mg- and/or Ca-rich material in soils and/or seawater

Rather than reducing the area footprint of material mined for CDR, another approach is to disperse it more widely. Grinding ultramafic or mafic basaltic rock reactants to smaller sizes than typical of mine tailings, and spreading them in agricultural soil, forest soil, or along beaches has been suggested as a means for carbon dioxide removal from air (e.g., Schuiling and Krijgsman, 2006). These ideas have recently been experimentally evaluated and reviewed in several papers (Beerling et al., 2018; Edwards et al., 2017; Hartmann et al., 2013; Kantola et al., 2017; Köhler et al., 2013; Köhler et al., 2010; Meysman and Montserrat, 2017; Montserrat et al., 2017; Moosdorf et al., 2014; Renforth and Henderson, 2017; Renforth et al., 2015; Rigopoulos et al., 2018b; Taylor et al., 2017; Taylor et al., 2016; ten Berge et al., 2012). Many of these studies use olivine as the reactant, because brucite and fibrous serpentine are not abundant in most candidate rock formations, fibrous serpentine (asbestos) is a health hazard, and most other serpentine minerals are slow to react at surface conditions. Some studies also consider basaltic lava as a reactant.

Carbon uptake in soils occurs through the interaction of air with dissolved alkalinity, which in some cases is known to release Ca at rates of 10^{-15} to 10^{-16} mol/cm^2/s (Renforth et al., 2015). The reaction of seawater with olivine ground to about 1 μm has comparable rates (Köhler et al., 2013; Montserrat et al., 2017; Rigopoulos et al., 2018b). Note that studies of mineral addition to seawater do not generally invoke precipitation of carbonate minerals, but rather charge balance of dissolved Mg^{2+} and/or Ca^{2+} via dissolution of atmospheric CO_2 as $2HCO_3^-$. Using the approach of Renforth (2012), an energy cost of $0.05 to $0.15 per kWh, and $10/ton for mining and crushing olivine to tailings size, without accounting for capital costs, efficiency and so on, we derive a minimum cost estimate for this method of approximately $25 to $52/ton.

Returning our focus to processes that produce carbonate minerals, Renforth et al. (2009, 2015) have shown that carbonate precipitation in

soil at brownfield sites modified with demolition rubble is 3 times higher than the value of average C content in urban areas, corresponding to a storage potential of 30 ± 10^{-2} kg CO_2/m^2. This increase in carbonate precipitation is attributed to the leaching of alkalinity from Ca-rich building materials that are pulverized during demolition to increase the reactive surface area and mix within the top layer of soil. Microbial processes may enhance weathering rates in soil, because microbial degradation of organic matter generates chelating agents and organic and inorganic acids. These microbial processes also accelerate mineral carbonation by increasing the local CO_2 partial pressure to 10–100 times atmospheric concentration (Power et al., 2010; Power et al., 2013a). These studies suggest that incorporating finely ground ultramafic and mafic rocks in agricultural soils or broadcasting rock material into the surface ocean may be sufficiently fast and inexpensive to be competitive with DAC systems. However, compared with the tailings methods described at the outset of this section, it may be difficult to measure and monitor the amount and fate of carbon stored in soils, beaches and seawater, and to distinguish natural carbon storage from that induced by engineered methods.

Carbon mineralization is often suggested as a method for mitigating the asbestos hazard posed by existing ultramafic mine tailings (e.g. McCutcheon et al., 2015); mining serpentinized, asbestos-bearing peridotite for the purpose of CO_2 removal from air could be a double-edged sword. Another significant concern in agricultural applications is that minor constituents in peridotite and serpentinite, such as Ni and Cr, could accumulate in soil or water over time. Oxidized Ni and Cr compounds in water and food constitute significant health hazards at low concentrations (US Environmental Protection Agency, 2017). For example, Beerling et al. (2018) wrote: “Weathering experiments reveal a fast release of bioavailable Ni from olivine …; experimental work with a soil column dosed with olivine suggested accumulation of Ni and Cr in the soil profile”. Similarly, Amann et al. (2020) report results of experiments on enhanced weathering of olivine added to agricultural soils indicating that “Ni and Cr are elevated in the soil solution, while Ni concentrations exceed the limits of drinking water quality”. In this context, basaltic rocks (containing higher molar ratios of (Mg + Ca)/Ni and (Mg + Ca)/Cr) may be more appropriate for use in agriculture. The addition of basaltic rock may also increase biomass yield, reduce nitrous oxide emissions, stabilize soil organic carbon content, replace of material lost through soil erosion, and enhance drought, salinity, heat, pest and disease resistance of plants (Beerling et al., 2018).

On the other hand, Hamilton et al. (2018) found that “trace metals are not present at detectable levels within [ultramafic] mine pit waters”. These observations are consistent with our own, previously unpublished measurements of Ni and Cr concentration in surface, spring and well water affected by natural weathering of ultramafic rocks in Oman (Table 1). As noted by Hamilton et al., the difference between the observations in this paragraph, and data on accumulation in soils, is probably due to the buffering capacity of ultramafic rocks and tailings, in which alteration assemblages contain abundant mineral hosts for Ni and Cr.

4. In situ CDR

In situ CDR – via circulation of CO_2-bearing surface water in appropriate formations to form subsurface carbonate minerals – has much lower surface area requirements compared to surficial CDR, but remains a largely speculative alternative.

Kinetic studies (reviews in NA19, Kelemen et al., 2011, Gadikota et al., 2020) suggest that in situ carbon mineralization in ultramafic rocks (with high molar Mg to Si ratios) and in glass-rich basaltic lava flows can form carbonate minerals accounting for tens of weight percent of CO_2 in the solid phase within a few years, when CO_2 is supplied by flowing pore fluid in an open system, over extensive rock volumes around individual boreholes. Experimental studies of reaction kinetics are consistent with the results of pilot experiments on carbon mineralization in mafic and ultramafic formations. For CDR, the challenge is to deliver CO_2 at a significant rate in order to take advantage of the relatively rapid carbon mineralization reactions.

It is important to add that a study estimating in situ carbon mineralization rates in a specific sandstone in a depleted oil reservoir (Benson et al., 2005) led to the widespread impression that this process is so slow that it would not become a significant factor for large scale storage of CO_2 until thousands of years after injection. However, this result is not applicable to carbon mineralization in basaltic lavas and ultramafic rocks, which can remove almost all CO_2 from circulating aqueous fluids in less than a year (Fig. 8).

4.1. In situ carbon mineralization in basalt

Storage of CO_2 captured elsewhere is not the focus of this paper. However, it is important to review results of field-scale, pilot experiments on storage of CO_2 via carbon mineralization. And, while the focus of this paper is not on carbon mineralization in basalt, we summarize the results of pilot experiments on storage in basalt, because there have been none in peridotite. Moreover, proposed hybrid methods for CDR, involving partial enrichment of CO_2 using direct air capture with synthetic sorbents (DACSS) coupled with injection of CO_2-rich water for in situ carbon mineralization (Section 5, Fig. 11 and associated text), very closely resemble the methodology used in the ongoing CarbFix experiment in Iceland and the recently completed Wallula Project in Washington State. Both involved extensive characterization of the composition, structure, and hydrology in thick sequences of basaltic lavas, followed by injection of CO_2-rich fluids to investigate storage in pore space and as solid carbonate minerals.

4.1.1. The Wallula project

The Wallula project (e.g., McGrail et al., 2017a; McGrail et al., 2017b; McGrail et al., 2014) injected 977 tons of water-saturated, supercritical CO_2 at a depth of 828 to 886 m into a relatively permeable horizon in the Columbia River basalt over a period of three weeks in summer 2013. Extensive surface monitoring and borehole observations for two years revealed no leakage of CO_2 from the highly permeable horizon into which it was injected. It is not known how much of the injected CO_2 is now stored as supercritical CO_2-rich fluid, dissolved in aqueous fluid, and/or stored in solid carbonate minerals. However, side cores from the main borehole wall revealed the presence of newly formed carbonate minerals precipitated by reaction of the basalt with injected CO_2, consistent with the composition of water in the borehole. Our understanding is that the project is complete with no plans for future work at this time.

4.1.2. The CarbFix experiment

The ongoing CarbFix experiment (e.g., Aradottir et al., 2011; Gislason et al., 2010; Gunnarsson et al., 2018; Matter et al., 2011; Matter et al., 2016; Snæbjörnsdóttir et al., 2017) is conducted by the geothermal power company Reykjavik Energy, together with a consortium of research scientists. In addition to investigating CO_2 storage, this project has the goal of storing H_2S co-produced with geothermal fluid at a specific power plant. Phase I of CarbFix injected about 200 tons of CO_2 into highly permeable, fractured basalts at a depth of 400–800 m (ambient temperature ~18–33 °C, porosity ~10%). At this depth, CO_2 solubility in water is not high, and CO_2 rich fluids are not supercritical. As a result, the project employed the novel technique of separately injecting H_2O and CO_2 with proportions adjusted to ensure complete solubility of CO_2 into aqueous fluid at the target depth. This technique is known as solution trapping. In CarbFix Phase I, water and CO_2 (± H_2S) were injected separately to a depth of 330–360 m, with an CO_2/H_2O ratio ~3.5 wt%. At this depth, CO_2 was “sparged” into the water as tiny bubbles, which were sufficiently small to be entrained in the descending water until they were entirely dissolved (Sigfusson et al., 2015).

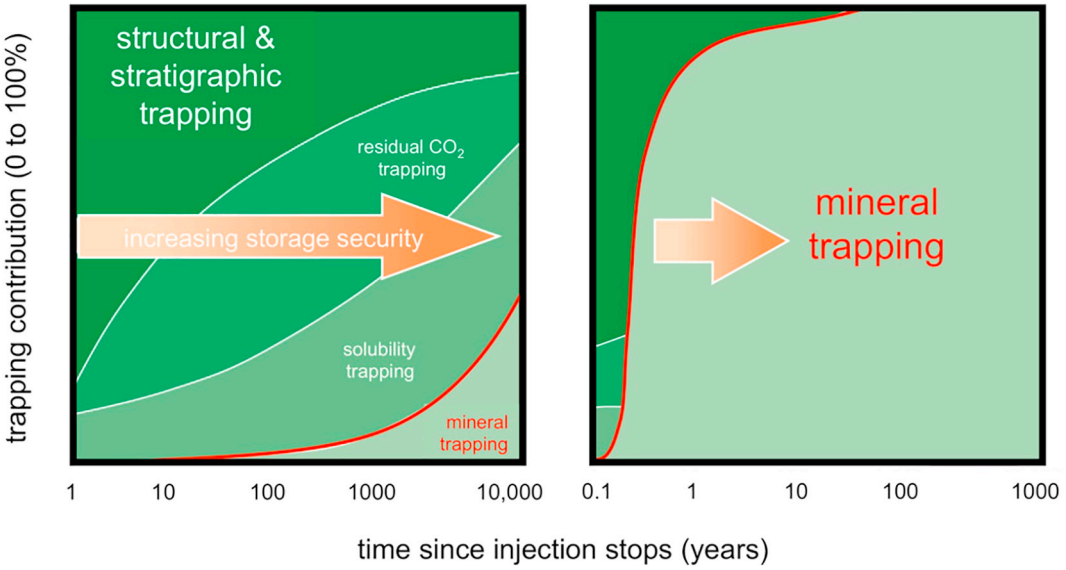

Fig. 8. Modified from Fig. 6.7 in NA19 (also, see Fig. 9 in Snæbjörnsdóttir et al., 2017). Lefthand panel, mechanisms of trapping injected, supercritical CO_2 from a typical sedimentary reservoir, after Krevor et al. (2015). Right hand panel, mechanisms of capturing and storing CO_2 introduced in aqueous fluids, in a peridotite or glassy basalt reservoir, approximated using data from NA19 and the results of the CarbFix experiment (described below).

CarbFix used a tracer technique, injecting SF_6 and other conserved tracers together with ^{14}C-rich CO_2. The tracers allowed researchers to see the injected fluid pulse arrive at production wells (Fig. 9), and to monitor the ratios of total carbon concentration, and ^{14}C, to the tracer concentrations. After an initial small pulse in ^{14}C at the production well, carbon concentration and ^{14}C in carbon returned to near-ambient levels. Carbon/tracer ratios, and ^{14}C/tracer ratios indicated >95% loss of carbon along the ~500 m flow path from injection to production well, attributed to carbon mineralization.

CarbFix Phase II is continuing with the methodology of Phase I, but with a deeper and wider range of injection depths (~1500 m at higher temperature), a reduction of the CO_2 injection pressure, and a large increase in CO_2 flux. Cumulatively, >20,000 tons of CO_2 have been injected, with tracer results continuing to indicate nearly complete loss of carbon along a ~2000 m flow path (Snæbjörnsdóttir et al., 2017). Phase II is close to the target scale for routine operation, accommodating most of Reykjavik Energy's CO_2 emissions at a specific geothermal power plant, and also disposing of H_2S produced at the power plant.

We estimated that the CO_2 uptake rate to date, in mass fraction per second, has been $\sim 10^{-11}$/s over three years (NA19). This figure corresponds to $\sim 5\ 10^{-9}$ mol/m^2/s if the rock reactants can be approximated as spheres 1 mm in diameter. This rate is similar to those calculated using experimental data on plagioclcase feldspar dissolution (Fig. 2) and experimental rates for full basalt carbonation (NA19). It is possible that the initial grain size of the most reactive minerals is <1 mm and/or that the surface area per grain is larger than it is for spheres. If so, the rate of CO_2 consumption in the CarbFix experiment may be limited by CO_2 supply, rather than the local reaction rate, and could be substantially higher if CO_2 were injected more rapidly.

The CarbFix methodology can be seen as a two-stage technique, first "solution trapping" of CO_2 dissolved in water at depth, almost instantaneously at the injection site, and then "mineral trapping" converting the dissolved CO_2 to solid carbonate over a period of a few months to years. If need be, carbon-depleted water could be produced downstream and recycled, reducing overall water consumption. Because of the first solution trapping step there is no requirement for an impermeable caprock to avoid CO_2 leakage. With an estimated cost of ~$20 to $50 per ton (Gunnarsson et al., 2018) this process costs ~$10 to $40/ton CO_2 more than injection of supercritical CO_2 into subsurface pore space for storage (NA19, Chapter 7), and could be a locally preferred option in some regions. This prospect opens vast expanses of potential basalt reservoirs for solid CO_2 storage.

There has been little focus on CDR via in situ carbon mineralization in basalt formations, due to relatively slow laboratory rates of carbon mineralization in basalt and minerals common in basalt (particularly plagioclase feldspar) compared to ultramafic rocks and their common minerals (e.g., olivine, asbestiform chrysotile, and brucite; Fig. 2 and NA19). However, the potential for CDR via rapid carbon mineralization in basaltic glass should not be overlooked.

4.2. *In situ carbon mineralization in peridotite and other ultramafic rocks*

4.2.1. *Geologic examples*

Geologic evidence for relatively rapid, natural carbon mineralization underlies proposed designs for engineered CDR systems. The classic paper of Barnes and O'Neil (1969) demonstrated that mantle peridotite near Earth's surface undergoes low temperature hydration (serpentinization) and carbonation at appreciable rates. The best studied natural example of this process is the alteration of mantle peridotite in the Samail ophiolite (e.g., Neal and Stanger, 1985), a block of oceanic crust and mantle peridotite thrust onto the Arabian continental margin from 96 to 70 million years ago, now exposed by faulting and erosion in northern Oman and the eastern United Arab Emirates. Present-day carbon mineralization forms carbonate veins in fractures, within partially serpentinized peridotites at ambient, near-surface temperature and pressure, and large travertine terraces of chemically-deposited calcite ($CaCO_3$) on the surface. Ongoing rates of carbonation, constrained by ^{14}C geochronology and other data, are on the order of 1 g CO_2/m^3/yr (1000 tons/km^3/yr) in a weathering horizon that may have an average depth of ~15 m (Kelemen and Matter, 2008; Kelemen et al., 2011; Mervine et al., 2014; Streit et al., 2012). Carbonates in the rock matrix and in veins filling fractures constitute about 1% of peridotite in outcrop, on average.

Carbonate veins are abundant in outcrops of mantle peridotite (e.g., Fig. 6.11 in NA19 Kelemen and Manning, 2015, Kelemen and Matter, 2008, Kelemen et al., 2011). Peridotite outcrops worldwide are also hosts to alkaline springs, rich in dissolved $CaOH^-$, with little dissolved Mg and C (e.g., Barnes et al., 1967; Barnes and O'Neil, 1969; Barnes and O'Neil, 1971; Barnes et al., 1978; Clark and Fontes, 1990; Falk et al., 2016; Kelley et al., 2001; Launay and Fontes, 1985; Mervine et al., 2014; Neal and Stanger, 1985). Alkaline spring waters are interpreted

as products of precipitation of Mg-carbonate minerals during reaction of groundwater with peridotite, together with dissolution of Ca-bearing silicates in peridotite (e.g., pyroxenes and plagioclase). At the surface, alkaline spring water combines directly with CO_2 from air to form calcium carbonate ($CaCO_3$) in travertine terraces (e.g., NA19, Fig. 6.12). ^{14}C data indicate that most of these large travertine deposits form in <50,000 years (Kelemen et al., 2019; Kelemen and Matter, 2008; Kelemen et al., 2011; Mervine et al., 2014). Similarly, ^{14}C data, together with conventional oxygen isotope mineral-fluid thermometry, clumped isotope thermometry, and phase equilibrium calculations indicate that carbonate veins in Oman peridotites are forming in the shallow subsurface as a result of ongoing weathering (e.g., Barnes and O'Neil, 1969; Kelemen et al., 2019; Kelemen and Matter, 2008; Kelemen et al., 2011; Malvoisin et al., 2020; Neal and Stanger, 1985; Streit et al., 2012). Thermodynamic modeling indicates that the alkaline spring waters in peridotite hosted catchments in Oman, California, Italy, and other localities form as a result of ongoing, subsurface precipitation of carbonate minerals + serpentine (e.g., Bruni et al., 2002; Paukert et al., 2012).

Fully carbonated peridotites (listvenites) are exposed in Oman. In listvenites, all Mg and Ca have combined with CO_2 to form carbonate minerals, while Si remains in the pure SiO_2 minerals quartz, chalcedony, and/or opal in Oman (Beinlich et al., 2020; Falk and Kelemen, 2015; Kelemen et al., 2020; Lacinska et al., 2014; Nasir et al., 2007; Stanger, 1985; Wilde et al., 2002) and elsewhere around the world (e.g., Akbulut et al., 2006; Azer et al., 2019; Beinlich et al., 2014; Beinlich et al., 2012; Borojević Šoštarić et al., 2014; Boschi et al., 2009; Gahlan et al., 2018; Garcia del Real et al., 2016; Halls and Zhao, 1995; Hansen et al., 2005; Menzel et al., 2018; Quesnel et al., 2016; Quesnel et al., 2013; Scarsi et al., 2018; Sofiya et al., 2017; Tominaga et al., 2017; Ulrich et al., 2014). In Oman, these listvenites formed about 90 million years ago at ~100–200 °C, in the presence of fluids with high P (CO_2) (Beinlich et al., 2020; de Obeso et al., 2017; Falk and Kelemen, 2015; Godard et al., 2017; Kelemen et al., 2017; Manning et al., 2017), similar to conditions for proposed in situ carbon mineralization. The presence of listvenites shows that there are natural pathways to complete reaction in this temperature range, despite potential negative feedbacks discussed in the next few paragraphs.

4.2.2. Feedbacks

In natural and engineered systems, rapid and extensive in situ carbon mineralization could be inhibited by negative feedback processes. Loss of CO_2 by reaction along the initial stages of a reactive fluid pathway could limit supply of CO_2 to rocks more distal from an injection well. Filling of pore space with reaction products may reduce permeability and armor reactive surfaces, forming a solid diffusive boundary layer between fluid and solid reactants. These negative feedbacks may commonly cause peridotite carbonation (and hydration and oxidation) to be self-limiting, preserving lithologies in outcrop that are far from equilibrium with surface conditions.

The reactions outlined in the Introduction all involve large increases in the solid volume, via addition of CO_2 ($\pm H_2O$, $\pm O_2$) from the fluid into the solid phases coupled with the low density of solid products relative to solid reactants. If large volumes of other components were dissolved from the rock volume, then perhaps the net change in solid volume would be small. However, nearly constant ratios of major cations (Mg/Si/Fe), compared to H_2O– and CO_2-free peridotite reactants, together with the results of thermodynamic calculations, indicate that there has been very little dissolution and transport of material out of the rock system (de Obeso and Kelemen, 2018; de Obeso et al., 2017; Kelemen et al., 2017; Malvoisin, 2015) consistent with decades of prior studies (e.g., Coleman and Keith, 1971) and with recent textural studies (Klein and Le Roux, 2020, Malvoisin et al., 2020). Thus, carbonation of ultramafic rocks, with or without concomitant hydration and oxidation, generally involves a large increase in the solid volume.

Near-surface peridotites have fracture-dominated porosity, on the order of ~1 vol%. In such a limited porosity network, small increases in the solid volume, and precipitation of minerals could have large, negative impacts on permeability, potentially limiting carbon mineralization in peridotite reacting with CO_2-rich fluids. Nevertheless, natural alkaline springs, formed as a result of subsurface peridotite carbonation and hydration, persist for tens of thousands to hundreds of thousands of years in Oman and on the seafloor (Früh-Green et al., 2003; Kelemen and Matter, 2008; Kelemen et al., 2011; Ludwig et al., 2006; Ludwig et al., 2011; Mervine et al., 2014; Mervine et al., 2015), indicating that the underlying reactive flow network does not clog or exhaust reactive surface area on this time scale. Similarly, as noted in the previous sub-section, 4.2.1, ^{14}C data, together with conventional oxygen isotope mineral-fluid thermometry, clumped isotope thermometry, and phase equilibrium calculations indicate that carbonate veins in Oman peridotites are forming in the shallow subsurface as a result of ongoing weathering. And, the presence of listvenites indicates that complete carbonation can occur.

A positive feedback mechanism that may explain the persistence of geologically rapid peridotite carbonation, extending over long times and to 100% completion, is “reaction-driven cracking” in which volume expansion due to carbonation causes large differential stresses, which in turn cause fractures, maintaining or enhancing permeability and reactive surface area (e.g, NA19, Fig. 6.14, Evans et al., 2018, Evans et al., 2020, Jamtveit et al., 2008, Jamtveit et al., 2009, Kelemen and Hirth, 2012, MacDonald and Fyfe, 1985, O'Hanley, 1992, Rudge et al., 2010, Ulven et al., 2014a, Ulven et al., 2014b). Available chemical potential energy to drive reaction-driven cracking in peridotite undergoing carbonation or hydration is large, more than sufficient to fracture rocks (Kelemen and Hirth, 2012). The overall concept seems simple enough, and this process has been observed in peridotite carbonation experiments (Zhu et al., 2016) and particularly well documented in analog experiments on hydration of MgO (Zheng et al., 2019; Zheng et al., 2018).

Nevertheless, in other experimental tests of olivine carbonation and hydration volume change and fractures were not observed (van Noort et al., 2017), and permeability dropped with increasing reaction progress (Andreani et al., 2009; Godard et al., 2013; Hövelmann et al., 2012; Lisabeth et al., 2017b). The reasons for this are not yet clear. It is becoming apparent that micro- and nano-scale properties of fluid-rock systems, such as fluid-mineral surface energy, and related characteristics such as sorptivity and disjoining pressure (Evans et al., 2018; Lambart et al., 2018; Zheng et al., 2018) may play a significant role in locating the crucial bifurcation between self-limiting negative feedbacks (clogging) and accelerating, positive feedbacks (cracking). In addition, viscous and/or frictional dissipation of stress, for example in weak reaction products such as gypsum (Skarbek et al., 2018) and brucite (Moore and Lockner, 2004; Moore and Lockner, 2007; Morrow et al., 2000; Zheng et al., 2019; Zheng et al., 2018), may also reduce crystallization pressure before stresses due to volume expansion become high enough to generate new fractures.

Other processes—such as selective, local dissolution and precipitation processes (Lisabeth et al., 2017b; Peuble et al., 2018) and/or crack propagation from etch pits along dislocation boundaries and other defects in olivine crystals (Daval et al., 2011; Klein et al., 2015; Lisabeth et al., 2017a; Lisabeth et al., 2017b; Malvoisin et al., 2017; McCollom et al., 2016; Plümper et al., 2012; Velbel, 2009) – may also play a role in sustaining permeability and fluid flow. Perhaps complete carbonation in natural systems is relatively slow, and thus cannot be engineered on a human time scale, as suggested by van Noort et al., 2017. However, in the competition between (i) volume expansion and stress accumulation, and (ii) processes that relax elastic stresses such as viscous flow or frictional sliding along existing fractures, it seems likely that reaction-driven cracking happens when the rates of reaction and volume change are maximized.

In summary, despite the initial, apparent simplicity of the feedbacks in peridotite carbonation, understanding them and developing

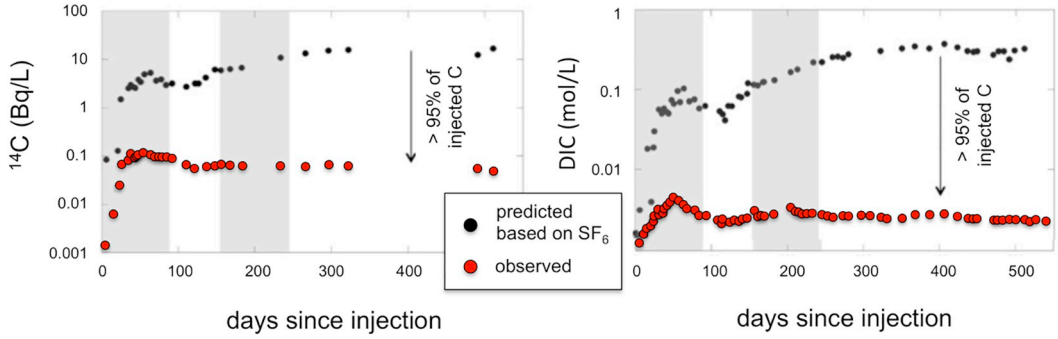

Fig. 9. Predicted and observed concentration and isotope ratio of carbon in water at the CarbFix Phase I production well. Predicted values are based on conservative tracers such as SF_6. The observed deficit in carbon concentration and ^{14}C are consistent with loss of consumption of almost all injected CO_2 along the flow path to form solid carbonate minerals.
(modified from Matter et al., 2016).

predictive hypotheses validated by experimental and field data is an increasingly complex and interesting research field. Continued research on this topic is justified by geologic observations of fully carbonated peridotite. Natural systems do it, and it is likely to be possible to design engineered systems that emulate the natural process. Moreover, understanding of the feedbacks that lead to reaction-driven cracking could be applied to geothermal power generation, in situ mining for, e.g., uranium, and extraction of oil and gas from tight reservoirs, as well as to CO_2 capture and storage. In other applications, it is desirable to prevent reaction-driven cracking, for example in well-bore cement and in caprocks above storage reservoirs for supercritical CO_2 fluid. Ongoing research seeks to outline a "phase diagram" delineating the conditions for reaction-driven cracking, and the surrounding parameter space dominated by clogging and armoring of reactive surfaces.

4.2.3. Engineered methods for CDR via carbon mineralization

Carbon dioxide removal from air, in addition to solid storage, may be achieved using engineered methods that closely emulate natural carbon mineralization in peridotite. During weathering, shallow ground water, equilibrated with atmospheric CO_2 reacts with peridotite in the subsurface, in a system closed to CO_2 exchange with the atmosphere. This quickly reduces dissolved carbon concentrations to zero, via precipitation of Mg- and Ca-carbonate minerals in veins. Along the reaction path, pH rises to 11.5 or more, and the concentration of dissolved Ca^{2-} increases to ~400 ppm. When these alkaline waters reach the surface, they combine with atmospheric CO_2 to form calcite, $CaCO_3$, in some places creating extensive travertine deposits (e.g., Barnes and O'Neil, 1969; Barnes et al., 1978; Clark and Fontes, 1990; Kelemen and Matter, 2008; Kelley et al., 2001; Launay and Fontes, 1985; Mervine et al., 2014).

Engineered CO_2 removal from air could begin with production of C-depleted alkaline water from existing aquifers in peridotite, to form travertine at the surface. The amount of CO_2 that could be captured via this simple and relatively inexpensive method is uncertain, because the size, permeability, productivity and recharge rates of alkaline, peridotite-hosted aquifers are unknown. This represents an obvious, relatively low-cost research opportunity.

In parallel, alkaline aquifers could be replenished via enhanced circulation of surface water through subsurface peridotite formations. Kinetic data yield empirical predictions of olivine carbonation rates (mass fraction olivine ≤75 μm) such as (Kelemen and Matter, 2008):

$$\Gamma = 1.15 \quad 10^{-5}\,(\mathrm{P(CO_2)\ bars})^{1/2} \exp[-0.000334(\mathrm{T°Ç} - 185)^2] \tag{9}$$

an expression that is consistent with more recent experimental results (Eikeland et al., 2015; Gadikota et al., 2014; Gadikota et al., 2020).

Rather than guess the effective grain size (and/or fracture spacing) in natural peridotite aquifers, we use observed rates in the near-surface weathering horizon as a calibration point, calculate relative rate enhancements using this expression, and derive a scaled rate from the product of the observed rate and the relative rate enhancement. This approach indicates that olivine-rich peridotite could, in principle, consume >1 Gt CO_2/km^3 peridotite/yr, at temperatures greater than ~150 °C, and CO_2 partial pressures greater than ~60 bars (Kelemen and Matter, 2008). Even at somewhat lower temperatures and CO_2 pressures, ~100 °C, carbon mineralization in peridotite reacting with aqueous fluid injected into a 10^7 m^3 volume of rock around a borehole at 3 km depth could achieve rates of ~0.05 Mt CO_2/yr for fluid saturated in air (400 ppmv CO_2) at 300 bars, or 0.5 Mt CO_2/yr for fluid saturated in air pre-enriched by partial DACSS to 5 wt% CO_2 at 300 bars. However, under some circumstances these kinetically achievable rates are likely to be limited by CO_2 supply, due to the costs and physical limitations of injecting fluid fractured peridotite aquifers at depth.

Carbon-species are dilute in water equilibrated with air at 1 bar. For example, there is ~100 ppm CO_2 equivalent (all dissolved inorganic C treated as CO_2) in seawater (Zeebe and Wolf-Gladrow, 2001) and in Mg-HCO_3-rich groundwater in peridotite aquifers (e.g., Bruni et al., 2002; Canovas et al., 2017; Paukert et al., 2012; Paukert Vankeuren et al., 2019). As a result, every penny spent pumping a given mass of water corresponds to ~$100 for the equivalent mass of CO_2, because $0.01 per mass of water must be divided by the mass fraction of 100 ppm CO_2 (10^{-4}) in that mass of water in order to calculate the cost per equivalent mass of CO_2. Thus, when using in situ carbon mineralization to capture CO_2 from dilute, aqueous solutions, it may be best to rely on thermal convection to drive fluid circulation. In this context, the temperature contrast between surface water and the target aquifer, and the permeability of the subsurface peridotite aquifer, are critical variables. Calculations presented by Kelemen et al. (2016) have been improved and updated as follows. Steady state, constant radial flux of fluid from a porous (fractured) aquifer into a borehole (Dake, 1978) can be quantified as

$$\text{`}Q = k2\pi rh/\mu \frac{dP}{dr} \text{ in a cylinder,} \quad \text{so that } dP = Q\mu/k2\pi h_p \frac{dr}{r}, \tag{10}$$

$$\text{and } P_Q = P_{wf} - P_e = Q\mu/k2\pi h_p \ln\left(\frac{r_w}{r_e}\right) \tag{11}$$

where Q is flux (m^3/s), k is permeability (m^2), A is area (m^2), μ is viscosity (Pa s), P is pressure (Pa), r is radial distance from the borehole (m), h is vertical distance or height (m), dP/dr is the radial pressure gradient from the borehole into the surrounding rock (Pa/m), h_p is the height of an interval in the borehole with perforated casing, P_{wf} is the fluid pressure at the bottom of the borehole, r_w is the radius of the borehole, P_e is the far-field fluid pressure in the formation, r_e is the critical radius at which the far-field fluid pressure is unchanged by the borehole, and P_Q is the excess fluid pressure required to produce a given flux. Ignoring transient effects on permeability due to drilling, this

expression can be used to estimate the excess fluid pressure required to achieve a given flux into or out of the borehole.

In addition, friction in the pipe can limit fluid flux. The additional pressure required to offset this frictional head loss (C.E.D. Engineering, 2019, Moody, 1944) is

$$P_f = \rho_{avg} g f (h_b)/(2r_w)\left\{\left(\frac{Q}{\pi r_w^2}\right)^2/(2g)\right\} \quad (12)$$

in which ρ_{avg} is the average fluid density (half the sum of minimum and maximum densities), g is the acceleration due to gravity (m/s^2), and f is a friction factor. The friction factor is first estimated for completely turbulent flow as

$$f_1 = \left[1.14 + 2\log_{10}\left(\frac{2r_w}{\varepsilon}\right)\right]^{-2} \quad (13)$$

and then iteratively refined as

$$f_{2\ to\ n} = \left(-2\log_{10}\left[\frac{\varepsilon/2r_w}{3.7} + \frac{2.51}{R_e f_{n-1}^{0.5}}\right]\right)^{-2} \quad (14)$$

in which ε is a pipe roughness constant (4.5732 10^{-5} m for steel pipe) and R_e is the Reynolds number

$$R_e = 2Q\rho_{avg}/(\mu\pi r_w) \quad (15)$$

Fluid pressure to achieve a given flux can result from thermal buoyancy, or can be imposed by pumping. Thermal buoyancy can be quantified as

$$P_b = \Delta\rho g h_b \quad (16)$$

in which P_b is the pressure due to buoyancy, $\Delta\rho$ is the difference in fluid density over a given temperature interval (kg/m^3), and h_b is the height of an interconnected fluid column, which is the depth of the borehole for our purposes.

The densities of cold and hot fluid as a function of temperature and pressure were estimated assuming that the circulating fluid is pure water, as

$$\rho_T = \rho_{0\circ C,1\ bar}\frac{1}{(1+\beta T_{\circ C})(1-(P_{Pa}-10^5)/E_{Pa})} \quad (17)$$

in which $\rho_{0°C,1\ bar}$ is 999.8 kg/m^3, β is the coefficient of thermal expansion, and E is the bulk modulus. β and E were fit to data from Engineering ToolBox (2009) over the relevant range of temperature and pressure (0 to 140 °C,1 to 300 bars) as

$$\beta_{1/\circ C} = -5.6643\ 10^{-5} + 1.5452\ 10^{-5}\ T_{\circ C} - 1.3299\ 10^{-7}\ T_{\circ C}^2 + 6.038\ 10^{-10}\ T_{\circ C}^3 \text{ and} \quad (18)$$

$$E_{Pa} = 2.0122\ 10^9 + 1.3778\ 10^7\ T_{\circ C} - 1.9648\ 10^5\ T_{\circ C}^2 + 6.5455\ 10^2\ T_{\circ C}^3 + 7\ 10^5\ P_{bars} \quad (19)$$

There are many areas where the temperature at 3 km depth reaches or exceeds 120 °C (e.g., Blackwell et al., 2011) providing a source of thermal buoyancy. For example, for an average annual surface temperature of 10 °C and 120 °C at 3 km, $\Delta\rho \sim 100$ kg/m^3.

When $P_b > P_Q + P_f$, thermal buoyancy is more than sufficient to produce a given flux, and no pumping is necessary. Otherwise, pumping is required to enhance the borehole fluid pressure by

$$P_p = P_Q + P_f - P_b \quad (20)$$

where P_p is the pump pressure. The power, $\wp$ (W) required to produce the required pump pressure is

$$\wp = QP_p. \quad (21)$$

Air saturated, Mg-HCO_3-rich surface waters in peridotite catchments contain ~100 ppm CO_2 by weight (all dissolved inorganic carbon calculated as CO_2; e.g., Barnes and O'Neil, 1969; Neal and Stanger, 1985; Bruni et al., 2002; Paukert et al., 2012; Paukert Vankeuren et al., 2019). Similarly, using EQ3/6 software (Wolery, 1979; Wolery, 1992), we calculate that reaction of surface water with peridotite at the surface can increase the CO_2 content to ~200 ppm, after which the water will saturate in Ca-Mg-carbonate minerals. Continued reaction during circulation through subsurface porosity consumes almost all of the dissolved carbon and magnesium to produce Mg-bearing carbonates plus hydrous Mg-silicates such as serpentine. This reaction process also dissolves Ca silicates, producing alkaline waters rich in $Ca(OH)_2$. Upon return to the surface, dissolved $Ca(OH)_2$ in alkaline water reacts with atmospheric CO_2 to produce $CaCO_3$ (solid calcite) + H_2O, consuming 1 mol of atmospheric CO_2 per mole of dissolved Ca, and/or dissolved Ca $(HCO_3)_2$, consuming 2 mol of CO_2 per mole of dissolved Ca. Using the thermodynamic code PHREEQC (Parkhurst and Appelo, 2013), with an alkaline fluid containing 9.44 mmol dissolved Ca per kg of water and a pH of 12, these reactions are estimated to consume ~400 to 800 ppm atmospheric CO_2 per kg of alkaline water returned to the surface. Thus, the total consumption of atmospheric CO_2 via circulation of surface water through subsurface peridotite, followed by return of CO_2 depleted water to the surface, is 0.0005 to 0.0010 kg CO_2/kg surface water.

Permeability in fractured, crystalline rock near the Earth's surface varies widely on many spatial scales, with values ranging from 10^{-12} to 10^{-17} (e.g., Ingebritsen and Manning, 2010; Manning and Ingebritsen, 1999; Rutqvist, 2015). Studies of the stimulated heat reservoir for the Soultz geothermal experiment yield values in the high end of this range (Vogt et al., 2014; Vogt et al., 2012; Zhang et al., 2014). Permeability in partially serpentinized, fractured peridotite may average 10^{-14} m^2 on the catchment scale (Dewandel et al., 2005), 10^{-12} m^2 on scales of 10's to 100's of meters near the surface and/or in tectonically fractured rock, and can be 10^{-12} to 10^{-15} m^2 on the mm to cm scale in rocks with microscopic serpentine veins but without macroscopic fractures, based on numerical simulations of flow through porosity imaged with synchrotron X-ray tomography (Waiching Sun, personal communication) and measurements of porosity plus dry and seawater-saturated conductivity (Oman Drilling Project, Initial Results, 2019). For CO_2 removal from air and solid storage via in situ carbon mineralization, it would be wise to prospect for relatively high permeability volumes within a peridotite formation.

These relationships, a power cost of $0.06/kWh (current, utility-scale, onsite, no storage, cost from DOE Solar Energy Technologies Office, 2017), and the assumption that production of energy is nearly free of CO_2 emissions, can be used to estimate the cost to remove a given mass of atmospheric CO_2 per year via in situ carbon mineralization, using a borehole to produce water from a subsurface peridotite aquifer containing an existing CO_2-depleted, Ca-rich alkaline fluid. We assume that the aquifer is sufficiently large, and/or that physical (and chemical) recharge of the borehole from the aquifer can keep pace with the rate of fluid production, at steady state. Field experiments will be essential to evaluate this assumption.

In the example calculation illustrated in Fig. 10, we use a permeability range of 10^{-12} to 10^{-14} m^2, a surface temperature of 10 °C, a borehole depth of 3000 m with a diameter of 0.33 m (13 in.) and a cost of $3 M (Augustine et al., 2006; Bloomfield and Laney, 2005; Shevenell, 2012), a production interval or intervals with a total height h_p of 1000 m, a bottom temperature of 120 °C, a basal fluid pressure of 300 bars, a critical radius, r_e, of 1000 m, and CO_2 consumption at 0.0009 kg CO_2/kg produced water (0.09 wt% CO_2). The approximate values resulting from this calculation suggest that CO_2 removal from air, at up to 10,000 tons per year per borehole, could be achieved at a cost less than $100/ton CO_2 via circulation of surface water for peridotite formations with a permeability greater than or equal to 10^{-13} m^2.

Scaling up this process to remove and store 1 Gt CO_2 from air per year is possible, but daunting. At 1000 to 10,000 tons CO_2 per well per year, this would require 100,000 to 1 million wells. While at first this seems inconceivable, it is similar to the ~1 million, currently producing

oil and gas wells in the United States (US Energy Information Administration, 2018) providing yet another example of the common result that disposing of fossil fuel emissions requires infrastructure with a scale similar to that of fossil fuel extraction.

The space requirements for this process are large. After drilling and well completion, each well head might only require 100 m^2, leading to a total area estimate of only 10 to 100 km^2 to capture and store 1 Gt CO_2/yr. However, to be effective, we estimate that wells must be at least 250 m apart, yielding an area requirement of 62,500 m^2 per well, and a total area estimate of 6250 to 62,500 km^2 for 1 Gt CO_2/yr. For comparison, the exposed outcrop area of mantle peridotite in Oman and the UAE is ~5000 km^2, and the global outcrop area of peridotite on land is probably less than ~25,000 km^2, while the outcrop area of peridotite on the seafloor flanking slow-spreading mid-ocean ridges may be >400,000 km^2 (Kelemen et al., 2011).

5. Hybrid methods: DACSS + carbon mineralization

In this section we explore the potential for hybrid approaches combining *incomplete* enrichment of air to 5 wt% CO_2 using DACSS, combined with in situ carbon mineralization, with the idea that these hybrids may be less expensive, in terms of energy and area requirements, than either of the end-member technologies alone.

Previous workers have considered CDR using DACSS, combined with carbon mineralization in basalt for storage of CO_2, perhaps in remote areas such as Kerguelen Island in the southern Indian Ocean (Goldberg et al., 2013), where renewable energy resources (wind, solar) are abundant, but there is a limited demand for electricity. It seems to us that this approach combines expensive DAC technology, enriching gas to high CO_2 concentrations, with a relatively expensive storage technology (carbon mineralization is perhaps twice as costly as storage of supercritical CO_2 in subsurface pore space). Thus, we think production of concentrated CO_2 via DACSS, powered by renewable energy in remote areas, is more likely to be combined with storage in pore space, or with export of CO_2 for use elsewhere. In addition to producing a saleable commodity, the latter option provides a practical way to store and eventually export surplus renewable energy, e.g., solar energy on the Arabian Peninsula.

However in general, the work required for DAC is proportional to the end purity of the output gas or fluid, and to the proportion of CO_2 removed from air (e.g., Wilcox et al., 2017). For an end-purity of 2.5 to 10%, the work required (and thus the power cost) is >2.5 times lower than for an end purity >95%. Also, for low end-purity, there is very little dependence on the proportion removed, which can thus be >90% with little added cost.

To provide initial, quantitative estimates of the associated cost savings, here we evaluate the cost of DACSS for a technology-agnostic system to take CO_2 from atmospheric concentrations (400 ppm by volume, 620 ppm by weight) to 3 vol% (~5 wt%). Building on the analysis presented by Wilcox et al. (Wilcox et al., 2017) the model from which these costs were derived is based on an exponential regression associated with the relationship between outlet purity and percent capture of the system and energy, and then subsequently the linear relationship between the energy and the CAPEX of a given system. The energetic requirements were correlated to the those of well-documented carbon capture systems today[2] as a function of the outlet purity and the percent capture.

The energy was then divided into the required thermal energy (80% of total energy requirements) and electric energy (20% of total energy requirements). Thermal energy is often required for sorbent regeneration, while electric energy is typically needed for fans, pumps, and vacuum equipment. Based on the energy resource, the energy-specific operating costs of the system were then determined. The capital cost of the system was correlated to the operating energy (and cost). This allowed for an approximation of the annualized capital. Finally, the maintenance and labor operating costs were developed consistent with the analysis in NA19, Chapter 5, where the maintenance cost is 3% of the total capital requirements and the labor cost is 30% of the maintenance cost.

For a case using natural gas and grid electricity, with the same heat and electricity costs as used for MgO looping in McQueen et al. (2020), in turn almost 100% consistent with those used in NA19, Chapter 5, the cost of 60% capture at 3% outlet purity is $70/ton CO_2 captured and 92/ton CO_2 net removed.[3] Fig. 11 shows the relationship between the outlet purity and both the cost of capture and the cost of CO_2 net removed. It can be seen that at higher outlet purities, the cost of capture and the net removed cost both increase on account of increased energy requirements for the separation process. It is important to note that the emissions factor contributing to the cost of CO_2 net removed ranges

[2] These known DAC systems include: the solvent DAC system in NA19, the sorbent DAC system in NA19, the sorbent DAC system presented in Wilcox et al. (Wilcox J, Psarras P, Pilorgé H, McQueen N, Liguori S, He J, Yuan M, Woodall C, Kian K, Pierpoint L, Jurewicz J, Lucas JM, Jacobson R, Deich N. 2020. Part 3: Cost Analysis of Direct Air Capture and storage Coupled to Low-Carbon Energy Resources in the U.S." *Environmental Science & Technology, Review)*. Carbon Engineering's liquid solvent system Keith DW, Holmes G, St. Angelo D, Heidel K. 2018. A process for capturing CO2 from the atmosphere. *Joule* 2: 1573–94, Klaus Lackner's moisture swing adsorption system Lackner K. 2009. Capture of

(*footnote continued*)
Carbon Dioxide from ambient air. *European Physical Journal: Special Topics* 176: 93–106, solvent system analysis by Mazzotti, et al., Direct air capture of CO_2 with chemicals: optimization of a two-loop hydroxide carbonate system using a countercurrent air-liquid contactor. Clim. Change 118, 119–135 (2013), and IECM simulations for point source capture from NGCC and PC power plants Carnegie Mellon University, 2019. Integrated Environmental Control Model, https://www.cmu.edu/epp/iecm.

[3] Within NA19, Chapter 5, the costs associated with solid sorbent DAC are reported as $88–$228/tCO_2 captured and vary from $89–$887/tCO_2 net removed (based on varying energy resources for thermal energy and electricity requirements). These costs are based on capturing 60–75% CO_2 from air at 99% purity. The net removed cost for the same conditions, presented here (>$314/ton CO_2) is substantially higher than $89/t$CO_2$, which corresponds to cases in which solar electricity and solar-based thermal energy are used to meet the energy requirements, or in which nuclear energy is used to meet both electricity and thermal requirements. In the NA19 solid sorbent analysis, the authors used a wide variety of parameters for inputs such as adsorbent cost, lifetime, capacity, air velocity, adsorption/desorption time, mass transfer coefficient, etc., to develop five different scenarios. The values reported for solid sorbents in NA19, Table 5.11 correspond to the range from the low-cost scenario to the high-cost scenario. The low cost scenario used a combination of low-cost inputs (i.e., lower adsorbent cost, higher adsorbent capacity, longer adsorbent lifetime, etc.) that may not all be physically achievable in the same DAC system. When the technology is deployed and operating, these parameters can be tested. Meanwhile, the lower-bound estimates reported in NA19 may be considered long-term targets, but are not the costs realized of DAC today nor likely over the next decade. Learning by doing will allow for the focused RD&D efforts that will hopefully lead to the realization of the lower-bound estimates of DAC. Many of the cost reductions embodied in the NA19 low-cost scenario ($89/ton CO_2 net-removed, compared to >$314/ton in Table 2) would also reduce the cost for enrichment to 5 vol% reported here ($75/ton in Table 2). Further discrepancies between the values in Table 2 and those in NA19 may result from the calculation of the energy requirements for the system. The model used here is technology agnostic, considering the price and energy requirements of well-documented carbon capture technologies as a function of outlet purity and percent capture. Since this approach has been generalized, it is not directly representative of the lower cost estimates in NA19, since those were associated with a single technology. Finally, in the NA19 low-cost scenarios, the solid sorbent analysis showed the same cost of CO_2 captured for solar and nuclear energy sources as the natural gas and coal scenarios. The operating cost of the system is highly dependent on the cost of thermal energy and electricity. Based on the current cost of energy, the NA19 low-cost scenarios may underestimate the energy operating cost associated with the solar and nuclear scenarios and, subsequently, underestimate the minimum cost of CO_2 net removed.

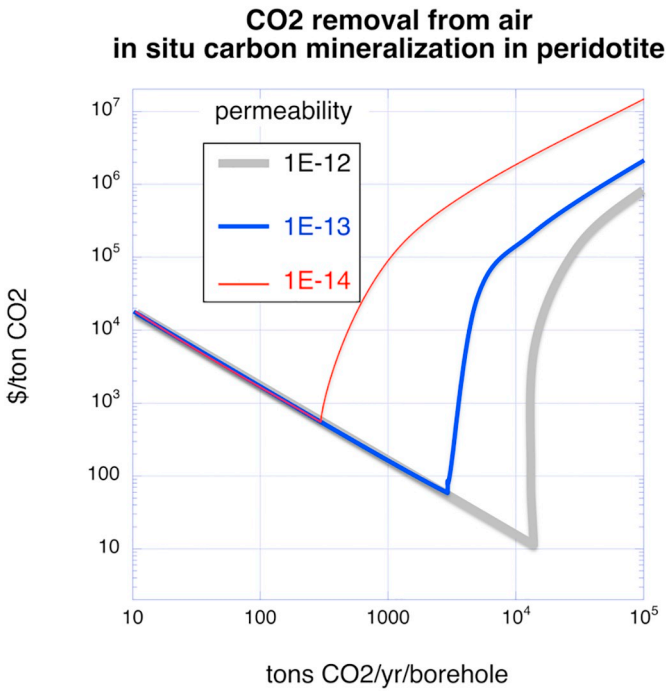

Fig. 10. Cost and rate of in situ carbon mineralization in peridotite, as a function of permeability (m^2).

from 0.25 tons CO_2 emitted/ton CO_2 captured at 3% outlet purity to 0.56 tons CO_2 emitted/ton CO_2 captured at 99.5% outlet purity. The image in Fig. 11 corresponds to results in Table 2.

Sparging of CO_2 enriched gas through "damp" MgO or heat-treated peridotite mine tailings would produce enhanced CO_2 uptake, compared to weathering of MgO in air. This kind of surficial, hybrid system was experimentally investigated by Harrison et al. (2012), who found that the rate of formation of solid Mg-carbonate from brucite ($Mg(OH)_2$) increased linearly as a function of increasing partial pressure of CO_2. As discussed in Section 4, this result would be similar for carbonation of MgO and heat-treated, serpentine-rich mine-tailings. MgO that would be completely carbonated in a year via weathering in air might be fully reacted in less than five days for MgO sparged with air enriched to 3 vol% CO_2. In turn, this could dramatically reduce the area requirement to remove a given mass of CO_2/yr from air via surficial weathering of MgO, heat-treated serpentine or ultramafic mine tailings. However, it would increase the area required for power generation for MgO-$MgCO_3$ looping by a similar factor.

We now turn to an analysis of the rate and cost of in situ carbon mineralization, using the same parameters as in Section 4.2.3, but assuming pre-equilibration of the circulating fluid with gas containing 3 vol% CO_2, rather than with air. As in CarbFix Phase II (Gunnarsson et al., 2018), sparging can be used to equilibrate the circulating fluid with CO_2-enriched gas. We use the method of Ogden et al. (2004), and an energy cost of $0.06/kWh, to estimate the cost of compressing air with 3 vol% CO_2 to a pressure of 2 to 10 bars for sparging, which is about $30 to $125/ton CO_2. Using seawater or Mg-HCO_3-rich water from peridotite aquifers greatly increases the solubility of carbon, compared to fresh water. We estimate that, using seawater, the sparging process will produce fluid containing 0.0055 to 0.0151 mol of C per liter, equivalent to 235 to 640 ppm CO_2 (values calculated using the thermodynamic model EQ3/6, Wolery, 1979, Wolery, 1992), compared to 0.002 to 0.003 mol of C per liter (88 to 130 ppm CO_2) in seawater equilibrated with air at 1 bar (EQ3/6 calculations and Zeebe and Wolf-Gladrow, 2001).

These relatively modest increases in seawater concentration, despite a factor of 160 to 800 increase in the partial pressure of CO_2, arise because C solubility (mainly as bicarbonate ion, HCO_3^-) is limited by the availability of charge-balancing cations (mainly, Mg^{2+} and Ca^{2+}). Additional enhancements in dissolved C concentration can be achieved by adding alkalinity. However, this is limited at high concentrations by saturation in carbonate minerals. Adding a commercially available base, such as NaOH or $NaHCO_3$ would probably be costly, per ton of CO_2 dissolved. Here, we calculate the effects of equilibrating water with heat-treated serpentine or ultramafic tailings or MgO as well as CO_2-enriched gas, in the kind of surficial process described two paragraphs previously. Calculated C concentrations produced by equilibration of water with an equal mass of serpentinized peridotite (average harzburgite, Hanghøj et al., 2010) plus gas with 3 vol% CO_2 at 2 to 10 bars are 0.0144 to 0.0277 mol per liter, equivalent to 600 to 1600 ppm CO_2. Calculations using MgO rather than peridotite produce a similar result.

Using a CO_2 concentration in circulating fluid of 1600 ppm for in situ carbon mineralization calculations, instead of 100 ppm in Section 4.2.3, yields lower costs per ton of CO_2, (for the in situ process alone) and higher rates of CO_2 uptake per borehole per year. Fig. 12 illustrates these costs, *including* the approximate cost of $65 for DAC enrichment of gas to 3 vol% CO_2 and $125/ton CO_2 for compression of CO_2-enriched gas to 10 bars prior to sparging in water for circulation through peridotite. In this hybrid DACSS – carbon mineralization scenario, our calculations suggest that CO_2 removal from air, at 8000 to 50,000 tons per borehole per year, could be achieved at a total cost less than $200/ton CO_2 via circulation of CO_2-enriched water through peridotite formations with a permeability between 10^{-12} and 10^{-13} m^2. In this hybrid case, scaling up this process to remove and store 1 Gt CO_2 from air per year would require 125,000 to 20,000 wells distributed over an area of 8000 to 1250 km^2, less daunting than the area requirement for in situ carbon mineralization alone.

Some key uncertainties require medium-scale field testing. In particular, the evolution of reaction progress and permeability during flow of fluid in a crystalline rock aquifer containing hierarchical fracture networks is difficult to predict. While modeling efforts are advisable, there really is no substitute for experiments at a scale that is tens to hundreds of times larger than the spacing of key fracture sets.

As is evident from data reviewed in NA19, the potential reservoir for CO_2 capture and storage in peridotite formations is enormous, with a capacity $>10^5$ Gt of CO_2. Both rates and costs of CO_2 capture from subsurface circulation of water saturated in air are potentially competitive with other methods to achieve carbon dioxide removal from air, and as a consequence proposed methods warrant intensified, basic research to delineate the conditions for cracking rather than clogging, and determine a variety of important physical properties of fractured, partially serpentinized, subsurface peridotite. Additionally, field tests should shed light on the potential for contamination of local water supplies, induced earthquakes, and other possible, negative impacts. Meanwhile, studies of natural peridotite weathering suggest that these impacts will be minimal, as discussed in Section 3.4. For example, Ni and Cr concentrations aquifers and springs within peridotite catchments are orders of magnitude lower than EPA limits for safe drinking water (Table 1). Similarly, Hamilton et al. (2020, 2018) found that Ni and Cr concentrations were below analytical detection limits in water associated with ultramafic mine pits and tailings. With regard to earthquakes, pilot CO_2 storage experiments in sedimentary reservoirs with similar permeabilities have not encountered a significant seismic hazard (NA19).

If pathways can be found to positive feedback regimes, then the cost of CDR and storage via in situ carbon mineralization in peridotite, and via hybrid combinations of DAC and in situ carbonation, could be relatively low (e.g., Figs. 10 and 12), comparable to estimated costs for nth-of-a-kind DAC with synthetic sorbents. And finally, in situ carbon mineralization driven by circulation of surface water through peridotite could be combined with geothermal power generation.

In the United States, potential sites for in situ CDR and storage in peridotite are abundant near both coasts (Krevor et al., 2009). In order

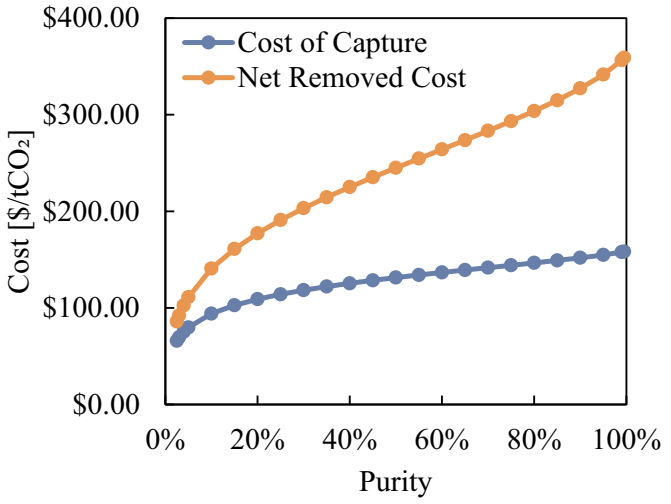

Fig. 11. Cost of direct air capture with synthetic sorbents (DACSS) as a function of purity at 60% capture. The cost of electricity (grid electricity) used is $0.06/kWh (NA19, US Energy Information Administration, 2020) and the cost of natural gas-derived thermal energy is $3.25/GJ (NA19). The emission from energy are 206 $kgCO_2$/GJ for grid electricity and 63 $kgCO_2$/GJ for natural gas thermal energy (NA19). The net removed cost shown in this image only incorporates the emissions associated with electric and thermal energy

to realize enhanced reaction rates at elevated temperature, areas of high heat flow are preferred, and these are localized in the western States. One of the largest peridotite massifs in north America, the Trinity peridotite in northern California, dips beneath the Cascade volcanic front (Fuis et al., 1987), an area of high heat flow with elevated temperatures at shallow depth (Bonner et al., 2003; Ingebritsen and Mariner, 2010), ideal for both geothermal power production and carbon mineralization in peridotite. Similarly, smaller bodies of peridotite flank the geothermal area in the Geysers region of northern California (Sadowski et al., 2016), near the Calpine power plant, which is the largest geothermal power plant in the world.

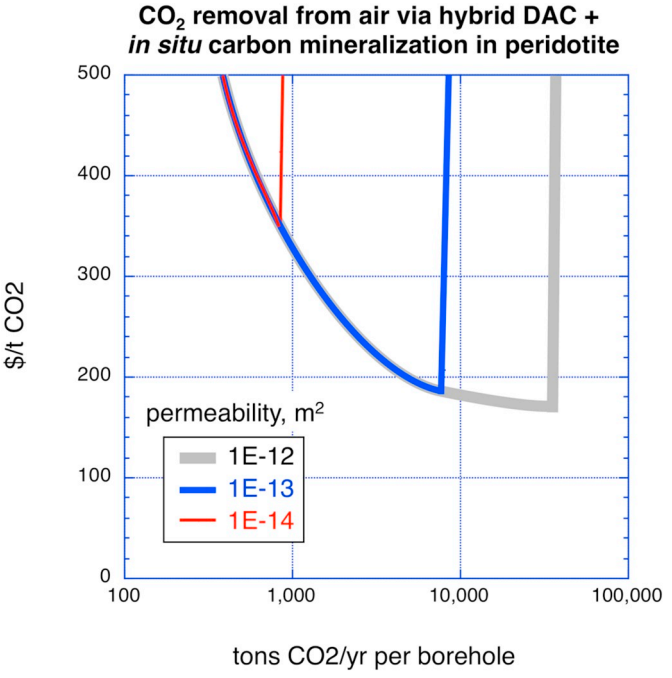

Fig. 12. Cost and rate of combined enrichment of air to 3 vol% (5 wt%) CO_2, followed by sparging of gas through peridotite-saturated water and in situ carbon mineralization in peridotite, as a function of permeability (m^2).

6. Research agenda

6.1. Carbon mineralization kinetics

For proposed surficial carbon mineralization, in which it is proposed to leave reactants exposed to the weather for a year or more, laboratory experiments are challenging due to slow reaction rates. However, the preliminary estimates in Section 3 suggest that surficial methods may be robust and relatively inexpensive, and this should drive experimental inquiry. An excellent set of experiments on low temperature brucite carbonation at a variety of CO_2 partial pressures (Harrison et al., 2012) allowed extrapolation to rates during weathering, providing an important check on long, difficult, direct determination of rates in air and surface water at ambient temperature. This could be a useful template for similar experiments on other materials. In particular, the rate of CO_2 uptake during weathering of caustic MgO could be very important, and is essentially unknown. Experimental and theoretical optimization of grain size for surficial carbon mineralization feedstock, minimizing grinding costs while maximizing rates, is another important area for laboratory, kinetic investigation.

NA19 contains a reasonably up-to-date compilation of carbon mineralization rates for different minerals, rock compositions and industrial wastes at elevated temperature and pressure, applicable to in situ carbon mineralization. Comparison of rates for different materials is still hampered by a lack of consistency in experimental methods, though Gadikota et al. (2020) provide a consistent set of experimental data for carbonation of olivine, plagioclase feldspar, basalt and a gabbroic rock ("anorthosite"). Recent work indicating rapid olivine hydration in the presence of high pH aqueous fluids (Andreani et al., 2013; Lafay et al., 2012) suggests that there should be renewed, systematic investigation of the effect of pH on carbon mineralization rates. The compilation is missing key data for carbon mineralization rates in alkaline industrial wastes. Producing a full matrix of experimental data for minerals, rocks and wastes, allowing comparison using units such as mol/(m^2 s), or mass fraction per second at a common grain size, at the same pressure, temperature and fluid composition, is a worthy research goal.

6.2. Chemo-mechanical feedbacks

Crystalline ultramafic rock tends to have low porosity and extensive fracturing. These characteristics create the potential for important feedbacks between carbon mineralization and permeability as discussed in Section 4.2.2. Consequently, extensive studies of chemo-mechanical processes are required to determine the conditions favoring reaction-driven cracking and other positive feedbacks, as well as the conditions leading to clogging of pore space and passivation via armoring of reactive surfaces. A crucial research goal is to create a "phase diagram" delineating the conditions favoring "cracking" versus "clogging" for carbon mineralization in ultramafic rocks.

If reaction-driven cracking were well understood, it would be possible to engineer conditions that generate ramified fracture networks at the grain scale. Such approaches could be valuable for a variety of technologies, including CO_2 capture and storage, geothermal power generation, in situ mining, and extraction of oil and gas from low permeability reservoirs. Similarly, avoiding reaction-driven cracking is important for ensuring the long-term integrity of impermeable cap rocks and well cement in boreholes for subsurface CO_2 and hydrocarbon reservoirs.

Increasingly, researchers are realizing that nano-scale material characteristics (mineral fluid surface energy, sorptivity, disjoining pressure) may play a key role in controlling the bifurcation between clogging and cracking. Because these characteristics vary in unpredictable ways from one material to another, research is moving away from simple analog systems (hydration or carbonation of CaO, MgO, and $CaSO_4$) toward experiments involving the most geologically

Table 1
Cr and Ni concentrations in water samples from peridotite-hosted surface water and aquifers in Oman. Paukert et al. (2012) and Paukert Vankeuren et al. (2019) describe methods of sample collection and analysis.

Sample ID	Site	Location	Zone 40Q Easting	Zone 40Q Northing	pH	ppb Cr	ppb Ni
Surface water and shallow groundwater samples							
OM10_06AI	Falej Al-Hallooh	Falej Al-Mar	0489581	2575531	8.52	1.7	<0.5
OM09_W06P	Nemo	Dima	0663140	2542366	8.84	3.3	1.6
OM10_01C	Wadi Input 1	Misbit	0625974	2576257	9.31	3.0	<0.5
OM10_01D	Wadi Input 2	Misbit	0625962	2576230	8.56	4.1	<0.5
OM09_W10W	15 Juergs up wadi	Misbit	0625674	2575981	8.66	4.2	<0.5
OM09_W08S	Aqueduct	Qafifah	0645906	2533393	8.99	3.2	<0.5
OM09_W09T	Waditorium	Qafifah	0645927	2533408	8.59	2.9	<0.5
OM10_04X	Palm Pool (fresh input)	Qafifah	0645784	2533424	8.94	0.6	2.0
OM09_W13E	Fresh pool	Shumayt	0486065	2588469	8.21	1.9	3.2
OM10_08AP	Audrey II	Shumayt	0486065	2588470	7.90	1.3	2.7
OM10_10AW	Edwin II	Uqaybah	0426225	2633900	8.49	<0.5	0.7
OM09_W11Y	Wadi Jahawif	Wadi Jahawif	0509861	2608158	8.71	1.7	0.5
OM09_W12B	Mohammed	Sudari	0442767	2649885	8.75	4.9	1.7
OM10_09AR	King Arthur	Sudari	0443057	2650131	8.76	3.7	0.7
OM10_11AX	SJA-4B	Peridotite borehole	0601942	2582989	7.23	9.0	2.7
OM10_11AY	SJA-4A	Peridotite borehole	0601962	2582964	7.57	9.1	0.6
OM10_12AZ	SJA-3B	Peridotite borehole	0602847	2582068	9.36	<0.5	<0.5
OM12_08Y	WDA-05 at 65 m	Peridotite borehole	0526133	2539283	9.052	4.3	<0.5
OM12_08Z	WDA-05 at 140 m	Peridotite borehole	0526133	2539283	9.108	5.2	<0.5
Hyperalkaline spring and borehole samples							
OM10_05AA	Aardvark	Al-Banah	0487584	2575976	11.65	<0.5	<0.5
OM09_W06O	Pacman	Dima	0663152	2542372	11.54	<0.5	<0.5
OM09_W04F	Lungs	Al Hilayw	0585584	2522988	11.76	<0.5	<0.5
OM10_10AV	Edwin I	Uqaybah	0426225	2633900	11.61	<0.5	<0.5
OM09_W02A	Falawj	Falaij	0608145	2525713	11.52	14.5	161.9
OM10_02L	Falej Source	Falaij	0608436	2525957	11.60	<0.5	<0.5
OM12_01G	Source	Falaij	0608145	2525713	11.25	<0.5	<0.5
OM10_03R	The Little Mermaid	North Falaij	0608561	2526486	11.63	<0.5	<0.5
OM10_06AG	Al-Thurawah	Falej Al-Mar	0489557	2575443	11.14	<0.5	<0.5
OM10_06AH	Al-Ohwenah	Falej Al-Mar	0489564	2575430	11.16	<0.5	<0.5
OM10_01A	Alkaline Spring Source	Misbit	0625997	2576261	11.29	<0.5	<0.5
OM09_W10U	Masibt spring	Misbit	0625710	2576013	11.37	6.6	25.5
0901117M	Glazed Kidney	Qafifah	646,115	2533648		0.8	0.8
OM10_04S	Glazed Kidney	Qafifah	646,115	2533648	11.76	<0.5	<0.5
090119Q	Eden	Qafifah	645,780	2533441		4.0	4.1
OM09_W07R	Dubya	Qafifah	0645857	2533372	11.63	<0.5	<0.5
OM10_07AJ	The Triangle	Shumayt	0486044	2588467	11.46	<0.5	<0.5
OM09_W13D	Triangle	Shumayt	0485756	2588221	11.45	<0.5	<0.5
OM10_09AT	Chain of Fools	Sudari	0443118	2650087	11.61	<0.5	<0.5
OM09_W12Z	Chain of Fools	Sudari	0442831	2649842	11.64	<0.5	<0.5
OM10_14BB	Red Well	Peridotite borehole	0612895	2605680	10.90	<0.5	<0.5
OM12_03M	NSHQ-14 at 15 m	Peridotite borehole	0675491	2529716	10.01	2.1	<0.5
OM12_03N	NSHQ-14 at 70 m	Peridotite borehole	0675491	2529716	11.03	<0.5	<0.5
OM12_03O	NSHQ-14 at 260 m	Peridotite borehole	0675491	2529716	11.05	<0.5	<0.5

relevant rock formations (e.g., peridotite and basalt for CO_2 capture and storage, shale for oil and gas, and sandstone for uranium). A growing community is working on these topics, inspired in part by the problems and promise of in situ mineral carbonation, and the dialog among different research groups around the world promises to be productive.

6.3. Field-scale pilot experiments

6.3.1. Surficial carbon mineralization

Based on extensive research by a few groups focused on this topic, surficial carbon mineralization for CDR and solid storage is ready for kiloton to megaton per year field experiments, together with extensive field inventories and laboratory characterization of the reactivity of various potential solid reactants. Field experiments on mine tailings and industrial wastes may be particularly good opportunities for university-industry and/or government-industry partnerships, as illustrated by a recently initiated collaboration involving the diamond-producer DeBeers and several academic research groups (Mervine et al., 2017). Significant limitations are the relatively small mass of accumulated and annually produced of mine-tailings, and the relatively limited CO_2 storage capacity of some industrial wastes with low concentrations of Mg and Ca. More effort needs to be focused on potential effects of geochemical contamination, because in many cases implementation is likely to be close to surface water and ground water resources. Carbonation of ultramafic mine tailings could be combined with efforts to reduce asbestos hazard at these sites, and carbonation of industrial wastes may also mitigate environmental hazards.

Progress on verification protocols and regulatory and pricing frameworks is another priority. Because of recent, damaging failures of tailings dams in the United States and Canada, the current regulatory and social environment discourages innovation in the design of tailings storage facilities. Creating a safe research space to explore innovation could ultimately lead to safer and more efficient operations. Funding could come from current and prospective industry partners.

Some work has focused on local modifications to ultramafic mine tailings, particularly mine tailings from highly altered serpentinites that include abundant brucite (and asbestiform chrysotile) (Alt et al., 2007; Assima et al., 2012; Assima et al., 2013a; Assima et al., 2013b; Assima et al., 2014a; Assima et al., 2014b; Assima et al., 2014c; Assima et al., 2014d; Bea et al., 2012; Hansen et al., 2005; Harrison et al., 2015; Harrison et al., 2016; Harrison et al., 2012; Larachi et al., 2010; Larachi et al., 2012; McCutcheon et al., 2015; Mervine et al., 2017; Power et al., 2009; Power et al., 2010; Power et al., 2016; Power et al., 2013a; Power et al., 2013b; Power et al., 2013c; Power et al., 2011; Power et al.,

2007; Pronost et al., 2012; Pronost et al., 2011; Savaramini et al., 2014; Thom et al., 2013; Wilson et al., 2010; Wilson et al., 2011; Wilson et al., 2009a; Wilson et al., 2014; Wilson et al., 2006; Wilson et al., 2009b). Suggested modifications are as simple as stirring tailings, depositing them in thinner layers, and sprinkling water on them to transport atmospheric CO_2 deeper into the pile for direct air capture. All of these ideas are simple enough to propose, but much work remains to conduct a set of pilot experiments that fill out the parameter matrix, especially considering the relatively long (annual-scale) times required.

Other suggested modifications are more innovative, and involve hybrid solutions incorporating both partial enrichment of CO_2 using direct air capture with synthetic sorbents (DACSS) and carbon mineralization. These include introducing CO_2-rich flue gas or fluid into slurry pipes that transport tailings. Two recent studies demonstrate the potential for up to a million-fold acceleration of carbon mineralization rates by sparging CO_2 rich gas through mine tailings (Assima et al., 2013a; Harrison et al., 2012). Their experiments achieved rates at ambient surface temperatures that approach or exceed the highest laboratory rates for carbon mineralization at elevated temperature and pressure, at least for CO_2 uptake of 3 to 10 wt%. Similar techniques might also be applied to alkaline industrial waste heaps. This is a promising avenue of research, which should be pursued in both laboratory experiments and field-scale pilot studies at several mine sites.

Carbon mineralization in crushed ultramafic materials may be viable in peridotite-rich alluvial gravels, which have high surface area to volume ratios and are present along some tectonic plate boundaries. A study of one ancient deposit found that it was already extensively carbonated (Beinlich et al., 2010). However, other basins with large volumes of peridotite gravel should be investigated to determine the extent to which they offer potential reactants for engineered carbon mineralization. For example, peridotite-rich sediments derived from mechanical weathering of the Samail ophiolite in Oman and the United Arab Emirates are present in km-thick formations beneath the Batinah coastal plain (e.g., Al Lazki et al., 2002) and in the extensive Barzaman Formation south and west of the ophiolite (Lacinska et al., 2014; Radies et al., 2004; Styles et al., 2006). While some of the ultramafic clasts in these rocks are extensively altered, subsurface exploration for less altered, more reactive potential CO_2 reservoirs in these settings is warranted.

6.3.2. *In situ CDR and carbon mineralization in ultramafic and mafic rocks*

It will be important to undertake two or three small- to medium-scale (~1 to 100 kt/year) field experiments. We envision multi-step pilot projects with gradually increasing cost, ambition, and risk, ideally with government and industry partners. Such projects will first require scoping efforts—characterizing physical properties and the suitability of rock formations for possible projects, and assessing the long term potential for significant CO_2 storage reservoirs. Scoping will also include a significant component of policy research, public outreach, and investigation of political and social factors in nearby communities and regions.

Once geologically and socially appropriate sites have been identified, pilot studies can be designed based on specific local opportunities. One generic first step might be to produce water from existing, alkaline, carbon-depleted aquifers for direct uptake of CO_2 from air to form travertine deposits on the surface, and increase the concentration of dissolved bicarbonate in surface water. The size, permeability, productivity, and physical and chemical recharge rates of peridotite-hosted, alkaline aquifers are unknown, and could readily be evaluated for several sites at a relatively low cost. Experiments could then progress to injecting recycled water into peridotite aquifers, with continued characterization of injectivity, permeability, volume, and subsurface rates of subsurface CO_2 mineralization. Pending a successful outcome of this step (CO_2 removal from circulating fluids, no sustained decrease in permeability), experiments could progress to investigating deeper circulation into hotter rock formations, with faster carbon mineralization rates. A final set of experiments could include injecting fluids with high CO_2 concentration to evaluate proposed storage of CO_2 captured elsewhere. The steps involving production and re-injection of ground water depend on government regulations, but might be relatively straightforward to implement.

The likely cost of such a phased experiment is estimated to increase from $1-3 M per year in the early stages, to $10 to $20 M per year when carried to the 100,000 to 1 M ton/year scale, based on the costs of CarbFix Phase I (Edda Aradottir, personal communication, 2017) and a notional budget for a large scale experiment on CO_2 storage in basalt (NA19, Appendix D, Table D.1). Because carbon mineralization rates in peridotite are optimal at ~185 °C, there is potential synergy between carbon mineralization and geothermal power generation. One good region to explore this synergy is northern California, where carbon management incentives and an active geothermal industry might facilitate combined government and industry participation.

6.4. *Process engineering*

There is considerable room for optimization of surficial methods, particularly MgO-$MgCO_3$ looping methods but also applicable to mine tailings in general, involving the energy source used for calcining, the area and thickness of reactive tailings fields used for weathering, the cost of potential stirring methods, the number of fields per calcining plant, the grain size of the tailings, and the time allowed for weathering, together with significant unknowns about reaction rates in different weathering environments, and the degradation or enhancement of materials during repeated cycles of weathering and calcining.

Similarly, there are many unknown parameters that are important for in situ carbon mineralization methods. These include optimizing the method and duration required for CO_2 uptake in CaOH-rich alkaline waters from peridotite aquifers, to draw down CO_2 from air, form solid calcium carbonate minerals for solid storage, and create CO_2-rich waters prior to circulation through subsurface peridotite. Though it may not be socially acceptable everywhere, use of hydrofracturing to enhance subsurface peridotite is another potential avenue for optimization of in situ methods.

For methods combining partial enrichment of CO_2 in air using DACSS with carbon mineralization, there are many additional opportunities for potential optimization, including specific methods for sparging CO2-bearing gas through tailings, for surficial carbon mineralization, or through peridotite-saturated water, prior to circulation through peridotite for in situ carbon mineralization.

7. Summary: Cost, capacity, potential and steps forward

Combined CO_2 removal from air (CDR) and solid storage, via surficial processes using existing ultramafic mine tailings, could be a relatively inexpensive and straightforward technology. Mining and crushing ultramafic rocks for the purpose CDR and storage may be cost-competitive with direct air capture systems using synthetic sorbents (DACSS), within the uncertainties for cost estimates for each type of process. The area footprint required is large, but both cost and area requirements can be greatly reduced by calcining carbonate reaction products, storing or selling CO_2, and re-using MgO and/or CaO to remove CO_2 from air via weathering. Similarly, in situ carbon mineralization, circulating CO_2-bearing aqueous fluid through subsurface fracture systems in ultramafic rocks, may be cost competitive with DACSS. Wells for in situ systems have a small footprint, but the requirement that wells must be far apart yields overall area requirements that are comparable to the total area of exposed mantle peridotite on land. Hybrid methods, using DACSS to enrich CO_2 to, e.g., 3%, combined with surficial and in situ carbon mineralization methods may reduce costs and area requirements compared to either of the end-member processes. Given the urgency to mitigate greenhouse gas emissions at scale, all of these avenues for mitigating CO_2 emissions via

carbon mineralization warrant continued, accelerated research programs, including laboratory experiments, numerical modeling, investigation of social and regulatory factors, environmental impacts, and field scale pilot projects.

Declaration of competing interest

All the authors except Vankeuren are inventors in Patent Application 62/865,708, "Systems and Methods for Enhanced Weathering and Calcining for CO_2 Removal from Air," filed by Columbia University on June 24, 2019. With others, Columbia University and Kelemen also hold US patents 8524152 & 9193594, "Systems and methods for enhancing rates of in situ carbonation of peridotite", and 20150129209A1 & 9657559B2, "Methods and systems for causing reaction driven cracking in subsurface rock formations". Kelemen currently serves as a consultant for The Jeremy and Hannelore Grantham Environmental Trust's "Neglected Climate Opportunities LLC", scoping sites for potential, field-scale pilot experiments on in situ carbon mineralization in peridotite.

Acknowledgements

We thank the two anonymous reviewers who worked hard to provide detailed, constructive reviews that substantially improved this long paper. We thank the National Academy committee who authored NA19, particularly the committee Chair, Steve Pacala, and those who presented at the committee meetings, particularly Edda Aradottir. The stimulating discussions of that committee continue to inspire and guide our research. Kelemen's effort on this paper and the underlying research has been supported by Alfred P. Sloan Foundation Grant 2014-3-01, NSF Research Grants EAR-1520732 and EAR-1516300, the International Continental Scientific Drilling Program (ICDP) Oman Drilling Project and Kelemen's Arthur D. Storke Chair at Columbia University. Wilcox and McQueen's efforts on this paper were supported in part by Prime Impact Fund. Renforth's contribution was supported by the UK Programme on Greenhouse Gas Removal (grants NE/P019943/1 and NE/P019730/1). Dipple is supported by a Discovery Grant from the Natural Sciences and Engineering Research Council of Canada. Mark Sonnenfeld kindly guided us to the petroleum engineering literature on calculating fluid flow in boreholes. We are very grateful to James Leong, Everett Shock, Dan McCorkle and Bob Anderson for providing a reality check on carbon solubility in water, particularly in sea water. Dan Sanchez was an enthusiastic and ambitious member of a breakout group discussing hybrid DAC + carbon mineralization methods at the Negative Emissions Technologies Workshop in Edinburgh in May 2019; without his insistence that we should develop something new and transformative, we might not have worked so hard on Section 5. Jürg Matter, Eric Oelkers, Alissa Park, Dave Goldberg and Julio Friedman provided advice on CO_2 storage via carbon mineralization at CarbFix, the history of MgO looping for CO_2 capture from flue gas, and the size of the CO2 utilization market. Roger Aines, Noah Deich, Larry Linden, Shashank Samala, Kevin Tidwell and Roger Ullman have been constant sources of encouragement and moral support.

References

Akbulut, M., Piskin, O., Karayigit, A.I., 2006. The genesis of the carbonatized and silicified ultramafics known as listvenites: a case study from the Mihaliccik region (Eskisehir), NW Turkey. Geol. J. 41, 557–580.

Al Lazki, A.I., Seber, D., Sandvol, E., Barazangi, M., 2002. A crustal transect across the Oman Mountains on the eastern margin of Arabia. GeoArabia 7, 47–78.

Alçiçek, H., 2009. Late Miocene nonmarine sedimentation and formation of magnesites in the Acıgöl Basin, southwestern Anatolia, Turkey. Sed. Geol. 219, 115–135.

Alt, J.C., Shanks, W.C., Bach, W., Paulick, H., Garrido, C.J., Beaudoin, G., 2007. Hydrothermal alteration and microbial sulfate reduction in peridotite and gabbro exposed by detachment faulting at the Mid-Atlantic Ridge, 15 degrees 20 ' N (ODP Leg 209): a sulfur and oxygen isotope study. G-Cubed 8.

Amann, T., Hartmann, J., Struyf, E., de Oliveira, Garcia W., Fischer, E.K., Janssens, I.A., Meire, P.M., Schoelynck, J., 2020. Enhanced weathering and related element fluxes: A cropland mesocosm approach. Biogeosciences 17, 103–119.

Andreani, M., Luquot, L., Gouze, P., Godard, M., Hoisé, E., Gibert, B., 2009. Experimental study of carbon sequestration reactions controlled by the percolation of CO2-rich brine through peridotites. Environ. Sci. Technol. 43, 1226–1231.

Andreani, M., Daniel, I., Pollet-Villard, M., 2013. Aluminum speeds up the hydrothermal alteration of olivine. Am. Min. 98, 1738–1744.

Aradottir, E.S.P., Sigurdardottir, H., Sigfusson, B., Gunnlaugsson, E., 2011. CarbFix: a CCS pilot project imitating and accelerating natural CO2 sequestration. Greenhouse Gases - Science and Technology 1, 105–118.

Assima, G.P., Larachi, F., Beaudoin, G., Molson, J., 2012. CO2 Sequestration in chrysotile mining residues: implication of watering and passivation under environmental conditions. Ind. Eng. Chem. Res. 51, 8726–8734.

Assima, G.P., Larachi, F., Beaudoin, G., Molson, J., 2013a. Dynamics of carbon dioxide uptake in chrysotile mining residues: effect of mineralogy and liquid saturation. Int. J. Greenhouse Gas Control 12, 124–135.

Assima, G.P., Larachi, F., Molson, J., Beaudoin, G., 2013b. Accurate and direct quantification of native brucite in serpentine ores—new methodology and implications for CO2 sequestration by mining residues. Thermochimica acta 566, 281–291.

Assima, G.P., Larachi, F., Molson, J., Beaudoin, G., 2014a. Comparative study of five Québec ultramafic mining residues for use in direct ambient carbon dioxide mineral sequestration. Chem. Eng. J. 245, 56–64.

Assima, G.P., Larachi, F., Molson, J., Beaudoin, G., 2014b. Emulation of ambient carbon dioxide diffusion and carbonation within nickel mining residues. Minerals Engineering 59, 39–44.

Assima, G.P., Larachi, F., Molson, J., Beaudoin, G., 2014c. Impact of temperature and oxygen availability on the dynamics of ambient CO2 mineral sequestration by nickel mining residues. Chem. Eng. J. 240, 394–403.

Assima, G.P., Larachi, F., Molson, J., Beaudoin, G., 2014d. New tools for stimulating dissolution and carbonation of ultramafic mining residues. Can. J. Chem. Eng. 92, 2029–2038.

Atashin, S., Wen, J.Z., Varin, R.A., 2015. Investigation of milling energy input on structural variations of processed olivine powders for CO2 sequestration. J. Alloys & Compounds 618, 555–561.

Augustine, C., Tester, J., Anderson, B., Petty, S., Livesay, B., 2006. A comparison of geothermal with oil and gas well drilling costs. In: Proc. 31st Workshop on Geothermal Reservoir Engineering. Stanford University SGP-TR-179.

Azer, M.K., Gahlan, H.A., Asimow, P.D., Mubarak, H.S., Al-Kahtany, K.M., 2019. Multiple stages of carbonation and element redistribution during formation of ultramafic-hosted magnesite in Neoproterozoic ophiolites of the Arabian-Nubian Shield, Egypt. Am. Min. 127, 81–107.

Baláž, P., Turianicová, E., Fabián, M., Kleiv, R.A., Briančin, J., Obut, A., 2008. Structural changes in olivine (Mg, Fe)2SiO4 mechanically activated in high-energy mills. Int. J. Mineral Processing 88, 1–6.

Balucan, R.D., Dlugogorski, B.Z., 2013. Thermal activation of antigorite for mineralization of CO2. Environ. Sci. Technol. 47, 182–190.

Balucan, R.D., Kennedy, E.M., Mackie, J.F., Dlugogorski, B.Z., 2011. Optimization of antigorite heat pre-treatment via kinetic modeling of the dehydroxylation reaction for CO2 mineralization. Greenhouse Gas Sci. Technol. 1, 294–304.

Barnes, I., O'Neil, J.R., 1969. Relationship between fluids in some fresh alpine-type ultramafics and possible modern serpentinization, western United States. GSA Bull. 80, 1947–1960.

Barnes, I., O'Neil, J.R., 1971. Calcium-magnesium carbonate solid solutions from Holocene conglomerate cements and travertines in Coast Range of California. Geochim. Cosmochim. Acta 35, 699.

Barnes, I., LaMarche, V.C., Himmelberg, G., 1967. Geochemical evidence of present-day serpentinization. Science 156, 830–832.

Barnes, I., O'Neil, J.R., Trescases, J.J., 1978. Present day serpentinization in New Caledonia, Oman and Yugoslavia. Geochim. Cosmochim. Acta 42, 144–145.

Bea, S.A., Wilson, S.A., Mayer, K.U., Dipple, G.M., Power, I.M., Gamazo, P., 2012. Reactive transport modeling of natural carbon sequestration in ultramafic mine tailings. Vadose Zone J. 11. https://doi.org/10.2136/vzj011.0053.

Beerling, D.J., Leake, J.R., Long, S.P., Scholes, J.D., Ton, J., Nelson, P.N., Bird, M., Kantzas, E., Taylor, L.L., Sarkar, B., Kelland, M., DeLucia, E., Kantola, I., Müller, C., Rau, G.H., Hansen, J., 2018. Farming with crops and rocks to address global climate, food and soil security. Nature Plants 4, 138–147.

Beinlich, A., Austrheim, H., Glodny, J., Erambert, M., Andersen, T.B., 2010. CO2 sequestration and extreme Mg depletion in serpentinized peridotite clasts from the Devonian Solund basin, SW-Norway. Geochim. Cosmochim. Acta 74, 6935–6964.

Beinlich, A., Plumper, O., Hovelmann, J., Austrheim, H., Jamtveit, B., 2012. Massive serpentinite carbonation at Linnajavri, N–Norway. Terra Nova 24, 446–455.

Beinlich, A., Mavromatis, V., Austrheim, H., Oelkers, E.H., 2014. Inter-mineral Mg isotope fractionation during hydrothermal ultramafic rock alteration – implications for the global Mg-cycle. Earth Planet Sci. Lett. 392, 166–176.

Beinlich, A., Plümper, O., Boter, E., Müller, I.A., Kourim, F., Ziegler, M., Harigane, Y., Lafay, R., Kelemen, P., Oman Drilling Project Science Team, 2020. Ophiolite carbonation: constraints from listvenite core BT1B, Oman Drilling Project. J. Geophys. Res In press.

Benson, S., Cook, P., Anderson, J., Bachu, S., Nimir, H.B., Basu, B., Bradshaw, J., Deguchi, G., Gale, J., von Goerne, G., Heidug, W., Holloway, S., Kamal, R., Keith, D., Lloyd, P., Rocha, P., Senior, B., Thomson, J., Torp, T., Wildenborg, T., Wilson, M., Zarlenga, F., Zhou, D., 2005. Underground geological storage. In: Metz, B., Davidson, O., Coninck, Hd, Loos, M., Meyer, L. (Eds.), IPCC Special Report on Carbon Dioxide Capture and Storage. Cambridge University Press, Cambridge, UK.

ten Berge, H.F., Van der Meer, H.G., Steenhuizen, J.W., Goedhart, P.W., Knops, P., Verhagen, J., 2012. Olivine weathering in soil, and its effects on growth and nutrient

uptake in ryegrass (*Lolium perenne* L.): a pot experiment. PloS One 7, e42098.
Blackwell, D., Richards, M., Frone, Z., Batir, J., Ruzo, A., Dingwall, R., Williams, M., 2011. Temperature-at-depth maps for the conterminous U.S. and geothermal resource estimates. GRC Transactions 35, 1545–1550.
Bloomfield, K.K., Laney, P., 2005. Estimating well costs for enhanced geothermal system applications. In: Idaho National Laboratory Report EXT-05-00660.
Bolen, W., 2020. Soda ash. In: USGS Mineral Commodity Summaries. US Geological Survey, pp. 152–153.
Bonner, J.L., Blackwell, D.D., Herrin, E.T., 2003. Thermal constraints on earthquake depths in California. Bull. Seismological Soc. Am. 93, 2333–2354.
Borojević Šoštarić, S., Palinkaš, A.L., Neubauer, F., Cvetković, V., Bernroider, M., Genser, J., 2014. The origin and age of the metamorphic sole from the Rogozna Mts., Western Vardar Belt: new evidence for the one-ocean model for the Balkan ophiolites. Lithos 192–195, 39–55.
Boschi, C., Dini, A., Dallai, L., Ruggieri, G., Gianellia, G., 2009. Enhanced CO2-mineral sequestration by cyclic hydraulic fracturing and Si-rich fluid infiltration into serpentinites at Malentrata (Tuscany, Italy). Chem. Geol. 265, 209–226.
Brantley, S., Chen, Y., 1995. Chemical weathering rates of pyroxenes and amphiboles. Rev. Min. Geochem. 31, 119–172.
Brantley, S., Mellott, N., 2000. Surface area and porosity of primary silicate minerals. Am. Min. 85, 1767–1783.
Bray, E.L., 2020. Magnesium compounds. USGS Mineral Commodity Summaries 100–101.
Brunauer, S., Emmett, P., Teller, E., 1938. Adsorption of gases in multimolecular layers. J. American Chem. Soc. 60, 309–319.
Bruni, J., Canepa, M., Chiodini, G., Cioni, R., Cipolli, F., Longinelli, A., Marini, L., Ottonello, G., Zuccolini, M.V., 2002. Irreversible water-rock mass transfer accompanying the generation of the neutral, Mg-HCO3 and high-pH, Ca-OH spring waters of the Genova province, Italy. Appl. Geochem. 17, 455–474.
C.E.D. Engineering, 2019. Spreadsheet Use for Pipe-flow Friction Factor Calculations. https://www.cedengineering.com/userfiles/Spreadsheet%20Use%20for%20Pipe%20Flow-Friction%20Factor%20Calculations.pdf.
Canovas, P.A., Hoehler, T., Shock, E.L., 2017. Geochemical bioenergetics during low-temperature serpentinization: an example from the Samail ophiolite, Sultanate of Oman. J. Geophys. Res. Biogeosci 122, 1821–1847.
Carnegie Mellon University, 2019. Integrated Environmental Control Model. https://www.cmu.edu/epp/iecm.
Caterpillar, 2018. Caterpillar Performance Handbook. https://wheelercat.com/company/resources/cat-performance-handbook/: (Caterpillar, Peoria, Illinois, U.S.A.).
Choi, H., Lee, W., Kim, S., 2009. Effect of grinding aids on the kinetics of fine grinding energy consumed of calcite powders by a stirred ball mill. Advanced Powder Technology 20, 350–354.
Clark, I.D., Fontes, J.C., 1990. Paleoclimatic reconstruction in northern Oman based on carbonates from hyperalkaline groundwaters. Quaternary Res. 33, 320–336.
Coleman, R.G., Keith, T.E., 1971. A chemical study of serpentinization, Burro Mountain, California. J. Petrol. 12, 311–328.
Curry, K.C., 2020. Wollastonite, Mineral Commodity Summaries, US Geological Survey. pp. 184–185.
Dake, L.P., 1978. Fundamentals of Reservoir Engineering, Developments in Petroleum Science. volume 8 Elsevier, Amsterdam (462 pp.).
Daval, D., Sissmann, O., Menguy, N., Saldi, G.D., Guyot, F., Martinez, I., Corvisier, J., Garcia, B., Machouk, I., Knauss, K.G., Hellmann, R., 2011. Influence of amorphous silica layer formation on the dissolution rate of olivine at 90°C and elevated pCO2. Chem. Geol. 284, 193–209.
Dewandel, B., Lachassagne, P., Boudier, F., Al-Hattali, S., Ladouche, B., Pinault, J.-L., Al Suleimani, Z., 2005. A conceptual hydrogeological model of ophiolite hard-rock aquifers in Oman based on a multiscale and a multidisciplinary approach. Hydrogeology 13, 708–726.
Dlugogorski, B.Z., Balucan, R.D., 2014. Dehydroxylation of serpentine minerals: implications for mineral carbonation. Renewable Sustain. Energy Rev. 31, 353–367.
DOE Solar Energy Technologies Office, 2017. 2020 Utility-scale Solar Goal Achieved. https://www.energy.gov/eere/solar/articles/2020-utility-scale-solar-goal-achieved.
Ebrahimi-Nasrabadi, K., Barati, M., Scott, P.W., 2013. Time-temperature-transformation (TTT) diagram of caustic calcined magnesia. In: 23rd World Mining Congress.
Edwards, D.P., Lim, F., James, R.H., Pearce, C.R., Scholes, J., Freckleton, R.P., Beerling, D.J., 2017. Climate change mitigation: potential benefits and pitfalls of enhanced rock weathering in tropical agriculture. Biology Letters 13, 20160715.
Eikeland, E., Blichfeld, A.B., Tyrsted, C., Jensen, A., Iversen, B.B., 2015. Optimized carbonation of magnesium silicate mineral for CO2 storage. ACS Applied Materials & Interfaces 7, 5258–5264.
Engineering ToolBox, 2009. Density of Liquids Versus Change in Pressure and Temperature. https://www.engineeringtoolbox.com/fluid-density-temperaturepressure-d_309.html.
Evans, O., Spiegelman, M.W., Kelemen, P.B., 2018. Reactive-brittle dynamics in peridotite alteration. J. Geophys. Res. 123, 8653–8675.
Falk, E.S., Kelemen, P.B., 2015. Geochemistry and petrology of listvenite in the Oman Ophiolite: complete carbonation of peridotite during ophiolite emplacement. Geochim. Cosmochim. Acta 160, 70–90.
Evans, O., Spiegelman, M., Kelemen, P.B., 2020. Phase-Field Modeling of Reaction-Driven Cracking: Determining Conditions for Extensive Olivine Serpentinization. J. Geophys. Res. 125 e2019JB018614.
Falk, E.S., Guo, W., Paukert, A.N., Matter, J.M., Mervine, E.M., Kelemen, P.B., 2016. Controls on the stable isotope compositions of travertine from hyperalkaline springs in Oman: insights from clumped isotope measurements. Geochim. Cosmochim. Acta 192, 1–28.
Fallick, A.E., Ilich, M., Russell, M.J., 1991. A stable isotope study of the magnesite deposits associated with the Alpine-type ultramafic rocks of Yugoslavia. Econ. Geol. 86, 847–861.
FAO The State of the World's Land and Water Resources for Food and Agriculture (SOLAW) – Managing Systems at Risk. available at. http://www.fao.org/3/a-i1688e.pdf (308 pp.).
Fedoročková, A., Hreus, M., Raschman, P., Sučik, G., 2012. Dissolution of magnesium from calcined serpentinite in hydrochloric acid. Minerals Engineering 32, 1–4.
Früh-Green, G.L., Kelley, D.S., Bernasconi, S.M., Karson, J.A., Ludwig, K.A., Butterfield, D.A., Boschi, C., Proskurowski, G., 2003. 30,000 years of hydrothermal activity at the Lost City vent field. Science 301, 495–498.
Fuis, G.S., Zucca, J.J., Mooney, W.D., Milkereit, B., 1987. A geologic interpretation of seismic refraction results in northeastern California. GSA Bull. 98, 53–65.
Gadikota, G., Matter, J., Kelemen, P.B., Park, A.-H.A., 2014. Chemical and morphological changes during olivine carbonation for CO2 storage in the presence of NaCl and NaHCO3. Physical Chemistry Chemical Physics 16, 4679–4693.
Gadikota, G., Fricker, K., Jang, S.-H., Park, A.-H., 2015. Carbonation of silicate minerals and industrial wastes and their potential use as sustainable construction materials. In: Jin, F., He, L.-N., Hu, Y.H. (Eds.), Advances in CO2 Capture, Sequestration, and Conversion, ACS Symposium Series. American Chemical Society, Washington DC.
Gadikota, G., Matter, J., Kelemen, P.B., Brady, P.V., Park, A.-H.A., 2020. Comparison of the carbon mineralization behavior of labradorite, anorthosite and basalt for CO2 storage. Fuel In press.
Gahlan, H.A., Azer, M.K., Asimow, P.D., 2018. On the relative timing of listwaenite formation and chromian spinel equilibration in serpentinites. Am. Min. 103, 1087–1102.
Garcia del Real, P., Maher, K., Kluge, T., Bird, D.K., Brown, G.E., John, C.M., 2016. Clumped-isotope thermometry of magnesium carbonates in ultramafic rocks. Geochim. Cosmochim. Acta 193, 222–250.
Gbor, P.K., Jia, C.Q., 2004. Critical evaluation of coupling particle size distribution with the shrinking core model. Chemical Engineering Science 59, 1979–1987.
Ghoorah, M., Dlugogorski, B.Z., Oskierski, H.C., Kennedy, E.M., 2014. Study of thermally conditioned and weak acid-treated serpentinites for mineralisation of carbon dioxide. Minerals Engineering 59, 17–30.
Gislason, S.R., Oelkers, E.H., 2003. Mechanism, rates and consequences of basaltic glass dissolution: II. An experimental study of the dissolution rates of basaltic glass as a function of pH and temperature. Geochim. Cosmochim. Acta 67, 3817–3832.
Gislason, S.R., Wolff-Boenisch, D., Stefansson, A., Oelkers, E., Gunnlaugsson, E., Sigurdardottir, H., Sigfusson, B., Broecker, W., Matter, J., Stute, M., Axelsson, G., Fridriksson, T., 2010. Mineral sequestration of carbon dioxide in basalt: the CarbFix project. Int. J. Greenhouse Gas Control 4, 537–545.
Godard, M., Luquot, L., Andreani, M., Gouze, P., 2013. Incipient hydration of mantle lithosphere at ridges: a reactive-percolation experiment. Earth Planet. Sci. Lett. 371–372, 92–102.
Godard M, Bennett E, Carter E, Kourim F, Lafay R, Noël J, Kelemen PB, Michibayashi K, Harris M. Oman Drilling Project Science Party, 2017. Geochemical and Mineralogical Profiles Across the Listvenite- Metamorphic Transition in the Basal Megathrust of the Oman Ophiolite: First Results From Drilling at Oman Drilling Project Hole BT1B. AGU Fall Meeting Abstracts. American Geophysical Union, 328591.
Goldberg, D., Lackner, K., Han, P., Slagle, A., Wang, T., 2013. Co-location of air capture, sub-ocean CO2 sequestration, and energy production on the Kerguelen plateau. Environ. Sci. Tech. 47, 7521–7529.
Gunnarsson, I., Aradóttir, E.S., Oelkers, E.H., Clark, D.E., Arnarsson, M.Þ., Sigfússon, B., Snæbjörnsdóttir, S.Ó., Matter, J.M., Stute, M., Júlíusson, B.M., Gíslason, S.R., 2018. The rapid and cost-effective capture and subsurface mineral storage of carbon and sulfur at the CarbFix site. Int. J. Greenhouse Gas Control 79, 117–126.
Halls, C., Zhao, R., 1995. Listvenite and related rocks: perspectives on terminology and mineralogy with reference to an occurrence at Cregganbaun, Co. Mayo, Republic of Ireland. Mineral. Deposita 30, 303–313.
Hamilton, J.L., Wilson, S.A., Morgan, B., Turvey, C.C., Paterson, D.J., Jowitt, S.M., McCutcheon, J., Southam, G., 2018. Fate of transition metals during passive carbonation of ultramafic mine tailings via air capture with potential for metal resource recovery. Int. J. Greenhouse Gas Control 71, 155–167.
Hamilton, J.L., Wilson, S.A., Morgan, B., Harrison, A.L., Turvey, C.C., Paterson, D.J., Dipple, G.M., Southam, G., 2020. Accelerating mineral carbonation in ultramafic mine tailings via direct CO2 reaction and heap leaching with potential for base metal enrichment and recovery. Econ. Geol. 115, 303–323.
Hanghøj, K., Kelemen, P.B., Hassler, D., Godard, M., 2010. Composition and genesis of depleted mantle peridotites from the Wadi Tayin massif, Oman ophiolite: major and trace element geochemistry, and Os isotope and PGE systematics. J. Petrol. 51, 206–227.
Hansen, L.D., Dipple, G.M., Gordon, T.M., Kellett, D.A., 2005. Carbonated serpentinite (listwanite) at Atlin, British Columbia: a geological analogue to carbon dioxide sequestration. Can. Mineral. 43, 225–239.
Harrison, A.L., Power, I.M., Dipple, G.M., 2012. Accelerated carbonation of brucite in mine tailings for carbon sequestration. Environ. Sci. Technol. 47, 126–134.
Harrison, A.L., Dipple, G.M., Power, I.M., Mayer, K.U., 2015. Influence of surface passivation and water content on mineral reactions in unsaturated porous media: implications for brucite carbonation and CO2 sequestration. Geochim. Cosmochim. Acta 148, 477–495.
Harrison, A.L., Dipple, G.M., Power, I.M., Mayer, K.U., 2016. The impact of evolving mineral–water–gas interfacial areas on mineral–fluid reaction rates in unsaturated porous media. Chem. Geol. 421, 65–80.
Hartmann, J., West, A.J., Renforth, P., Köhler, P., De La Rocha, C.L., Wolf-Gladrow, D.A., Dürr, H.H., Scheffran, J., 2013. Enhanced chemical weathering as a geoengineering strategy to reduce atmospheric carbon dioxide, supply nutrients, and mitigate ocean acidification. Rev. Geophys. 51, 113–149.
Haug, T.A., Kleiv, R.A., Munz, I.A., 2010. Investigating dissolution of mechanically

activated olivine for carbonation purposes. Applied Geochem. 25, 1547–1563.
Hepburn, C., Adlen, E., Beddington, J., Carter, E.A., Fuss, S., Dowell, N.M., Minx, J.C., Smith, P., Williams, C.K., 2019. Perspective: the technological and economic prospects for CO2 utilization and removal. Nature 575, 87–97.
Hövelmann, J., Austrheim, H., Jamtveit, B., 2012. Microstructure and porosity evolution during experimental carbonation of a natural peridotite. Chem. Geol. 334, 254–265.
Huijgen, W.J.J., Comans, R.N.J., Witkamp, G.-J., 2007. Cost evaluation of CO2 sequestration by aqueous mineral carbonation. Energy Convers. Management 48, 1923–1935.
Infomine, 2018. Mine Costs. http://costs.infomine.com/costdatacenter/miningcostmodel.aspx.
Ingebritsen, S.E., Manning, C.E., 2010. Permeability of the continental crust: dynamic variations inferred from seismicity and metamorphism. Geofluids 10, 193–205.
Ingebritsen, S.E., Mariner, R.H., 2010. Hydrothermal heat discharge in the Cascade Range, northwestern United States. J. Volc. Geotherm. Res. 196, 208–218.
IPCC, 2014. In: Core Writing Team, Pachauri, R.K., Meyer, L.A. (Eds.), Climate Change 2014: Synthesis Report. Contribution of Working Groups I, II and III to the Fifth Assessment Report of the Intergovernmental Panel on Climate Change. IPCC, Geneva, Switzerland 151 pp.. https://www.ipcc.ch/report/ar5/syr/.
IPCC, 2018. Global Warming of 1.5°C, Intergovernmental Panel on Climate Change. https://www.ipcc.ch/sr15/.
Jamtveit, B., Malthe-Sorenssen, A., Kostenko, O., 2008. Reaction enhanced permeability during retrogressive metamorphism. Earth Planet. Sci. Lett. 267, 620–627.
Jamtveit, B., Putnis, C., Malthe-Sorenssen, A., 2009. Reaction induced fracturing during replacement processes. Contrib. Mineral. Petrol. 157, 127–133.
Kantola, I.B., Masters, M.D., Beerling, D.J., Long, S.P., DeLucia, E.H., 2017. Potential of global croplands and bioenergy crops for climate change mitigation through deployment for enhanced weathering. Biology Letters 13, 20160714.
Keith, D.W., Holmes, G., St. Angelo, D., Heidel, K., 2018. A process for capturing CO2 from the atmosphere. Joule 2, 1573–1594.
Kelemen, P.B., Hirth, G., 2012. Reaction-driven cracking during retrograde metamorphism: olivine hydration and carbonation. Earth Planet. Sci. Lett. 345–348, 81–89.
Kelemen, P.B., Manning, C.E., 2015. Reevaluating carbon fluxes in subduction zones, what goes down, mostly comes up. Proc. Nat. Acad. Sci. 112, E3997–E4006. https://doi.org/10.1073/pnas.1507889112.
Kelemen, P.B., Matter, J., 2008. In situ mineral carbonation in peridotite for CO2 storage. Proc. National Acad. Sci. (US) 105 (17), 295–17,300.
Kelemen, P.B., Matter, J., Streit, E.E., Rudge, J.F., Curry, W.B., Blusztajn, J., 2011. Rates and mechanisms of mineral carbonation in peridotite: natural processes and recipes for enhanced, in situ CO2 capture and storage. Ann. Rev. Earth Planet. Sci. 39, 545–576.
Kelemen, P.B., Brandt, A.R., Benson, S.M., 2016. Carbon dioxide removal from air using seafloor peridotite. In: AGU Fall Meeting Abstracts. American Geophysical Union, GC21J-07.
Kelemen, P., de Obeso, J.C., Manning, C., Godard, M., Bach, W., Cai, M.Y., Choe, S., Coggon, J., Ellison, E., Eslami, A., Evans, K., Harris, M., Kahl, W.-A., Matter, J., Michibayashi, K., Okazaki, K., Pézard, P., Teagle, D.A.H., Templeton, A., Oman Drilling Project Science Team, 2019. Peridotite alteration in OmanDP cores. In: JpGU Abstracts. Japanese Geoscience Union, SCG49-03.
Kelemen, P.B., Godard, M., Johnson, K.T.M., Okazaki, K., Manning, C.E., Urai, J.L., Michibayashi, K., Harris, M., Coggon, J.A., Teagle, D.A.H., The Oman Drilling Project Phase I Science Party, 2017. Peridotite carbonation at the leading edge of the mantle wedge: OmDP Site BT1. In: AGU Fall Meeting Abstracts. American Geophysical Union, 328655.
Kelemen, P., Benson, S.M., Pilorgé, H., Psarras, P., Wilcox, J., 2019a. An overview of the status and challenges of CO2 storage in minerals and geological formations. Frontiers in Climate 1, 9.
Kelemen, P.B., Matter, J.M., Teagle, D.A.H., Coggon, J.A., Oman Drilling Project Science Team, 2020. Proceedings of the Oman Drilling Project. International Ocean Discovery Program, College Station, TX, doi:10.14379/Oman.ph1-2.proc.2020..
Kelley, D.S., Karson, J.A., Blackman, D.K., Fruh-Green, G.L., Butterfield, D.A., Lilley, M.D., Olson, E.J., Schrenk, M.O., Roe, K.K., Lebon, G.T., Rivizzigno, P., 2001. An off-axis hydrothermal vent field near the Mid-Atlantic Ridge at 30 degrees N. Nature 412, 145–149.
Klein, F., Grozeva, N.G., Seewald, J.S., McCollom, T.M., Humphris, S.E., Moskowitz, B., Berquó, T.M., Kahl, W.-A., 2015. Fluids in the crust: experimental constraints on fluid-rock reactions during incipient serpentinization of harzburgite. Am. Min. 100, 991–1002.
Klein, F., Le Roux, V., 2020. Quantifying the volume increase and chemical exchange during serpentinization. Geology In press.
Kleiv, R.A., Thornhill, M., 2006. Mechanical activation of olivine. Minerals Engineering 19, 340–347.
Köhler, P., Hartmann, J., Wolf-Gladrow, D.A., 2010. Geoengineering potential of artificially enhanced silicate weathering of olivine. Proc. Nat. Acad. Sci. 107 (20,228-20,33).
Köhler, P., Abrams, J.F., Völker, C., Hauck, J., Wolf-Gladrow, D.A., 2013. Geoengineering impact of open ocean dissolution of olivine on atmospheric CO2, surface ocean pH and marine biology. Environ. Res. Lett. 8, 014009.
Krevor, S.C., Graves, C.R., Van Gosen, B.S., McCafferty, A.E., 2009. Mapping the Mineral Resource Base for Mineral Carbon-dioxide Sequestration in the Conterminous United States: U.S. Geological Survey Digital Data Series 414, 14 p., 1 Plate. Only available at URL. http://pubs.usgs.gov/ds/414.
Krevor, S., Blunt, M.J., Benson, S.M., Pentland, C.H., Reynolds, C., Al-Menhali, A., Niu, B., 2015. Capillary trapping for geologic carbon dioxide storage: from pore scale physics to field scale implications. International Journal of Greenhouse Gas Control 40, 221–237.
Lacinska, A.M., Styles, M.T., Farrant, A.R., 2014. Near-surface diagenesis of ophiolite-derived conglomerates of the Barzaman Formation, United Arab Emirates: a natural analogue for permanent CO2 sequestration via mineral carbonation of ultramafic rocks. Geol. Soc. London Spec. Pub. 392, 343–360.
Lackner, K.S., Wendt, C.H., Butt, D.P., Joyce, E.L., Sharp, D.H., 1995. Carbon-dioxide disposal in carbonate minerals. Energy 20, 1153–1170.
Lafay, R., Montes-Hernandez, G., Janots, E., Chiriac, R., Findling, N., Toche, F., 2012. Mineral replacement rate of olivine by chrysotile and brucite under high alkaline conditions. J. Crystal Growth 347, 62–72.
Lambart, S., Savage, H.M., Kelemen, P.B., 2018. Experimental investigation of the pressure of crystallization of Ca(OH)2: implications for the reactive-cracking process. G-cubed 19. https://doi.org/10.1029/2018GC007609.
Larachi, F., Daldoul, I., Beaudoin, G., 2010. Fixation of CO2 by chrysotile in low-pressure dry and moist carbonation: ex-situ and in-situ characterizations. Geochim. Cosmochim. Acta 74, 3051–3075.
Larachi, F., Gravel, J.-P., Grandjean, B.P.A., Beaudoin, G., 2012. Role of steam, hydrogen and pretreatment in chrysotile gas–solid carbonation: opportunities for pre-combustion CO2 capture. Int. J. Greenhouse Gas Control 6, 69–76.
Launay, J., Fontes, J.-C., 1985. Les sources thermales de Prony (Nouvelle-Calédonie) et leurs précipités chimiques: Exemple de formation de brucite primaire. Géologie de la France 83–100.
Li, J., Hitch, M., 2017. Ultra-fine grinding and mechanical activation of mine waste rock using a planetary mill for mineral carbonation. Int. J. Mineral Processing 158, 18–26.
Li, W., Li, W., Li, B., Bai, Z., 2009. Electrolysis and heat pretreatment methods to promote sequestration by mineral carbonation. Chem. Eng. Res. Design 87, 210–215.
Lisabeth, H., Zhu, W., Xing, T., De Andrade, V., 2017a. Dissolution-assisted pattern formation during olivine carbonation. Geophys. Res. Lett. 44. https://doi.org/10.1002/2017GL074393.
Lisabeth, H.P., Zhu, W., Kelemen, P.B., Ilgen, A., 2017b. Experimental evidence for chemo-mechanical coupling during carbon mineralization in ultramafic rocks. Earth Planet Sci. Lett. 474, 355–367.
Ludwig, K.A., Kelley, D.S., Butterfield, D.A., Nelson, B.K., Früh-Green, G., 2006. Formation and evolution of carbonate chimneys at the Lost City hydrothermal field. Geochim. Cosmochim. Acta 70, 3625–3645.
Ludwig, K.A., Shen, C.-C., Kelley, D.S., Cheng, H., Edwards, R.L., 2011. U–Th systematics and 230Th ages of carbonate chimneys at the Lost City Hydrothermal Field. Geochim. Cosmochim. Acta 75, 1869–1888.
MacDonald, A.H., Fyfe, W.S., 1985. Rate of serpentinization in seafloor environments. Tectonophys. 116, 123–135.
Malvoisin, B., 2015. Mass transfer in the oceanic lithosphere: serpentinization is not isochemical. Earth Planet Sci. Lett. 430, 75–85.
Malvoisin, B., Brantut, N., Kaczmarek, M.-A., 2017. Control of serpentinization rate by reaction-induced cracking. Earth Planet Sci. Lett. 476, 143–152.
Malvoisin, B., Zhang, C., Müntener, O., Baumgartner, L.P., Kelemen, P.B., Oman Drilling Project Science Team, 2020. Measurement of volume change and mass transfer during serpentinisation: insights from the Oman Drilling Project. J. Geophys. Res In press.
Manning, C.E., Ingebritsen, S.E., 1999. Permeability of the continental crust: the implications of geothermal data and metamorphic systems. Rev. Geophysics 37, 127–150.
Manning, D.A.C., Renforth, P., Lopez-Capel, E., Robertson, S., Ghazireh, N., 2013. Carbonate precipitation in artificial soils produced from basaltic quarry fines and composts: an opportunity for passive carbon sequestration. International Journal of Greenhouse Gas Control 17, 309–317.
Manning, C.E., Kelemen, P.B., Michibayashi, K., Harris, M., Urai, J.L., de Obeso, J.C., Jesus, A.P.M., Zeko, D., Oman Drilling Project Science Party, 2017. Transformation of serpentinite to listvenite as recorded in the vein history of rocks From Oman Drilling Project Hole BT1B. In: AGU Fall Meeting Abstracts. American Geophysical Union, 328604.
Maroto-Valer, M.M., Fauth, D.J., Kuchta, M.E., Zhang, Y., Andresen, J.M., 2005. Activation of magnesium rich minerals as carbonation feedstock materials for CO2 sequestration. Fuel Processing Technology 86, 1627–1645.
Martins, S., 2016. Size–energy relationship in comminution, incorporating scaling laws and heat. Int. J. Mineral Processing 153, 29–43.
Matter, J.M., Broecker, W., Gislason, S.R., Gunnlaugsson, E., Oelkers, E., Stute, M., Sigurdardóttir, H., Stefansson, A., Wolff-Boenisch, D., Axelsson, G., Sigfússon, B., 2011. The CarbFix Pilot Project: storing carbon dioxide in basalt. Energy Procedia 4, 5579–5585.
Matter, J.M., Stute, M., Snaebjornsdottir, S.O., Oelkers, E.H., Gislason, S.R., Aradottir, E.S., Sigfusson, B., Gunnarsson, I., Sigurdardottir, H., Gunnlaugsson, E., Axelsson, G., Alfredsson, H.A., Wolff-Boenisch, D., Mesfin, K., Taya, D.F.D., Hall, J., Dideriksen, K., Broecker, W.S., 2016. Rapid carbon mineralization for permanent disposal of anthropogenic carbon dioxide emissions. Science 352, 1312–1314.
McCollom, T.M., Klein, F., Robbins, M., Moskowitz, B., Berquó, T.S., Jöns, N., Bach, W., Templeton, A., 2016. Temperature trends for reaction rates, hydrogen generation, and partitioning of iron during experimental serpentinization of olivine. Geochim. Cosmochim. Acta 181, 175–200.
McCutcheon, J., Dipple, G.M., Wilson, S.A., Southam, G., 2015. Production of magnesium-rich solutions by acid leaching of chrysotile: a precursor to field-scale deployment of microbially enabled carbonate mineral precipitation. Chem. Geol. 413, 119–131.
McGrail, B.P., Spane, F.A., Amonette, J.E., Thompson, C.R., Brown, C.F., 2014. Injection and monitoring at the Wallula Basalt Pilot Project. Energy Procedia 63, 2939–2948.
McGrail, B.P., Schaef, H.T., Spane, F.A., Cliff, J.B., Qafoku, O., Horner, J.A., Thompson, C.J., Owen, A.T., Sullivan, C.E., 2017a. Field validation of supercritical CO2

reactivity with basalts. Environ. Sci. Techol. Lett. 4, 6–10.
McGrail, B.P., Schaef, H.T., Spane, F.A., Horner, J.A., Owen, A.T., Cliff, J.B., Qafoku, O., Thompson, C.J., Sullivan, E.C., 2017b. Wallula Basalt Pilot Demonstration Project: post-injection results and conclusions. Energy Procedia 114, 5783–5790.
McKelvy, M.J., Chizmeshya, A.V.G., Diefenbacher, J., Bearat, H., Wolf, G., 2004. Exploration of the role of heat activation in enhancing serpentine carbon sequestration reactions. Environ. Sci. Technol. 38, 6897–6903.
McQueen, N., Kelemen, P.B., Dipple, G.M., Renforth, P., Wilcox, J., 2020. Ambient weathering of magnesium oxide for CO2 removal from air (CDR). Nature Communications In press.
Menzel, M.D., Garrido, C.J., López Sánchez-Vizcaíno, V., Marchesi, C., Hidas, K., Escayola, M.P., Delgado, Huertas A., 2018. Carbonation of mantle peridotite by CO2-rich fluids: the formation of listvenites in the Advocate ophiolite complex (Newfoundland, Canada). Lithos 323, 238–261.
Mervine, E.M., Humphris, S.E., Sims, K.W.W., Kelemen, P.B., Jenkins, W.J., 2014. Carbonation rates of peridotite in the Samail Ophiolite, Sultanate of Oman constrained through 14C dating and stable isotopes. Geochim. Cosmochim. Acta 126, 371–397.
Mervine, E.M., Sims, K.W.W., Humphris, S.E., Kelemen, P.B., 2015. Applications and limitations of U-Th disequilibria systematics for determining rates of peridotite carbonation in the Samail Ophiolite, Sultanate of Oman. Chem. Geol. 412, 151–166.
Mervine, E.M., Dipple, G.M., Power, I.M., Wilson, S.A., Southam, G., Southam, C., Matter, J.M., Kelemen, P.B., Stienhofer, J., Miya, Z., 2017. Potential for offsetting diamond mine carbon emissions through mineral carbonation of processed kimberlite. In: 11th International Kimberlite Conference Abstracts. University of Alberta Library, 11IKC-4553.
Meysman, F.J., Montserrat, F., 2017. Negative CO2 emissions via enhanced silicate weathering in coastal environments. Biology Letters 13, 20160905.
Mitina, N.A., Lotov, V.A., Sukhushina, A.V., 2015. Influence of heat treatment mode of various magnesia rocks on their properties. Procedia Chemistry 15, 213–218.
Montserrat, F., Renforth, P., Hartmann, J., Leermakers, M., Knops, P., Meysman, F.J., 2017. Olivine dissolution in seawater: implications for CO2 sequestration through Enhanced Weathering in coastal environments. Environ. Sci. Tech. 51, 3960–3972.
Moody, L.F., 1944. Friction factors for pipe flow. Trans ASME November, 671–684.
Moore, D.E., Lockner, D.A., 2004. Crystallographic controls on the frictional behavior of dry and water-saturated sheet structure minerals. J. Geophys. Res. 109, B03401.
Moore, D.E., Lockner, D.A., 2007. Comparative deformation behavior of minerals in serpentinized ultramafic rock: application to the slab-mantle interface in subduction zones. Int. Geol. Rev. 49, 401–415.
Moosdorf, N., Renforth, P., Hartmann, J., 2014. Carbon dioxide efficiency of terrestrial enhanced weathering. Environ. Sci. Tech. 48, 4809–4816.
Morrow, C.A., Moore, D.E., Lockner, D.A., 2000. The effect of mineral bond strength and adsorbed water on fault gouge frictional strength. Geophys. Res. Lett. 27, 815–818.
Mortsell, S., Svensson, J., 1951. Discussion of a paper entitled: a new surface measurement tool for mineral engineers, by F.W. Bloecher, Jr. Trans. AIME 190, 981–983.
Nasir, S., Al Sayigh, A., Al Harthy, A., Al-Khirbash, S., Al-Jaaidi, O., Musllam, A., Al-Mishwat, A., Al-Bu'saidi, S., 2007. Mineralogical and geochemical characterization of listwaenite from the Semail Ophiolite, Oman. Chemie der Erde 67, 213–228.
National Academies of Sciences Engineering and Medicine, 2019. Negative Emissions Technologies and Reliable Sequestration: A Research Agenda. The National Academies Press, Washington DC. https://doi.org/10.17226/25259. (495 pp.).
Neal, C., Stanger, G., 1985. Past and present serpentinization of ultramafic rocks: an example from the Semail ophiolite nappe of northern Oman. In: Drewer, J.I. (Ed.), The Chemistry of Weathering. D. Reidel Publishing Company, Holland, pp. 249–275.
van Noort, R., Wolterbeek, T.K.T., Drury, M.R., Kandianis, M.T., Spiers, C.J., 2017. The force of crystallization and fracture propagation during in-situ carbonation of peridotite. Minerals 7. https://doi.org/10.3390/min7100190.
de Obeso, J.C., Kelemen, P.B., 2018. Fluid rock interactions in residual mantle peridotites overlain by shallow oceanic limestones: insights from Wadi Fins, Sultanate of Oman. Chem. Geol. 498, 139–149.
de Obeso, J.C., Kelemen, P.B., Manning, C.E., Michibayashi, K., Harris, M., Oman Drilling Project Science Party, 2017. Listvenite formation from peridotite: insights from Oman Drilling Project hole BT1B and preliminary reaction path model approach. In: AGU Fall Meeting Abstracts. American Geophysical Union, 328802.
O'Connor, W.K., Dahlin, D.C., Rush, G.E, Gerdemann, S.J., Penner, L.R., Nilsen, D.N., 2005. Final Report: Aqueous Mineral Carbonation—Mineral Availability, Pretreatment, Reaction Parametrics, And Process Studies. DOE/ARC-TR-04-002 Office of Process Development, National Energy Technology Laboratory, Office of Fossil Energy, US Department of Energy, Albany, OR.
Ogden, J.M., Yang, C., Johnson, N., Ni, J., Johnson, J., 2004. Conceptual Design of Optimized Fossil Energy Systems With Capture and Sequestration of Carbon Dioxide, Appendix B, CO2 Compression …, Final Report, DOE Award DE-FC26-02NT41623. https://escholarship.org/content/qt4nx7p2rz/qt4nx7p2rz.pdf.
O'Hanley, D.S., 1992. Solution to the volume problem in serpentinization. Geology 20, 705–708.
Palandri, J.L., Kharaka, Y.K., 2004. Open File Report 2004-1068: A Compilation of Rate Parameters of Water-Mineral Interaction Kinetics for Application to Geochemical Modeling. US Geological Survey.
Pan, S.-Y., Chang, E.E., Chiang, P.-C., 2012. CO2 capture by accelerated carbonation of alkaline wastes: a review on Its principles and applications. Aerosol & Air Quality Res. 12, 770–791.
Parkhurst, D.L.Appelo, C.A.J. Description of Input and Examples for PHREEQC Version 3: A Computer Program for Speciation, Batch-reaction, One-Dimensional Transport, And Inverse Geochemical Calculations: Book 6, Chapter. A43. available only at. http://pubs.usgs.gov/tm/06/a43.
Paukert Vankeuren, A., Matter, J.M., Stute, M., Kelemen, P.B., 2019. Multitracer determination of apparent groundwater ages in peridotite aquifers within the Samail Ophiolite, Sultanate of Oman. Earth Planet Sci. Lett. 516, 37–48.
Paukert, A.N., Matter, J.M., Kelemen, P.B., Shock, E.L., Havig, J.R., 2012. Reaction path modeling of enhanced in situ CO2 mineralization for carbon sequestration in the peridotite of the Samail Ophiolite, Sultanate of Oman. Chem. Geol. 330, 86–100.
Peuble, S., Andreani, M., Gouze, P., Pollet-Villard, M., Reynard, B., Van de Moortele, B., 2018. Multi-scale characterization of the incipient carbonation of peridotite. Chem. Geol. 476, 150–160.
Plümper, O., Røyne, A., Magrasó, A., Jamtveit, B., 2012. The interface-scale mechanism of reaction-induced fracturing during serpentinization. Geology 40, 1103–1106.
Pohl, W., 1990. Genesis of magnesite deposits: models and trends. Geologische Rundschau 79, 291–299.
Power, I.M., Wilson, S.A., Thom, J.M., Dipple, G.M., Southam, G., 2007. Biologically induced mineralization of dypingite by cyanobacteria from an alkaline wetland near Atlin, British Columbia, Canada. Geochem. Transactions 8. https://doi.org/10.1186/467-4866-8-13.
Power, I.M., Dipple, G.M., Southam, G., 2009. The hydromagnesite playas of Atlin, British Columbia, Canada: a biogeochemical model for CO2 sequestration. Chemical Geology 260, 286–300.
Power, I.M., Dipple, G.M., Southam, G., 2010. Bioleaching of ultramafic tailings by Acidithiobacillus spp. for CO2 sequestration. Environ. Sci. Technol. 44, 456–462.
Power, I.M., Wilson, S.A., Small, D.P., Dipple, G.M., Wan, W., Southam, G., 2011. Microbially mediated mineral carbonation: roles of phototrophy and heterotrophy. Environ. Sci. Technol. 45, 9061–9068.
Power, I.M., Harrison, A.L., Dipple, G.M., Southam, G., 2013a. Carbon sequestration via carbonic anhydrase facilitated magnesium carbonate precipitation. Int. J. Greenhouse Gas Control 16, 145–155.
Power, I.M., Harrison, A.L., Dipple, G.M., Wilson, S.A., Kelemen, P.B., Hitch, M., Southam, G., 2013b. Carbon mineralization: From natural analogues to engineered systems. Rev. Min. & Geochem. 77, 205–260.
Power, I.M., Wilson, S.A., Dipple, G.M., 2013c. Serpentinite carbonation for CO2 sequestration. Elements 9, 115–121.
Power, I.M., Harrison, A.L., Dipple, G.M., 2016. Accelerating mineral carbonation using carbonic anhydrase. Environ. Sci. Technol. 50, 2610–2618.
Pronost, J., Beaudoin, G., Tremblay, J., Larachi, F., Duchesne, J., Hebert, R., Constantin, M., 2011. Carbon sequestration kinetic and storage capacity of ultramafic mining waste. Environ. Sci. Technol. 45, 9413–9420.
Pronost, J., Beaudoin, G., Lemieux, J.-M., Hebert, R., Constantin, M., Marcouiller, S., Klein, M., Duchesne, J., Molson, J.W., Larachi, F., Maldague, X., 2012. CO2-depleted warm air venting from chrysotile milling waste (Thetford Mines, Canada): evidence for in-situ carbon capture from the atmosphere. Geology 40, 275–278.
Quesnel, B., Gautier, P., Boulvais, P., Cathelineau, M., Maurizot, P., Cluzel, D., Ulrich, M., Guillot, S., Lesimple, S., Couteau, C., 2013. Syn-tectonic, meteoric water–derived carbonation of the New Caledonia peridotite nappe. Geology 41, 1063–1066.
Quesnel, B., Boulvais, P., Gautier, P., Cathelineau, M., John, C.M., Dierick, M., Agrinier, P., Drouillet, M., 2016. Paired stable isotopes (O, C) and clumped isotope thermometry of magnesite and silica veins in the New Caledonia Peridotite Nappe. Geochim. Cosmochim. Acta 183, 234–249.
Radies, D., Preusser, F., Matter, A., Mange, M., 2004. Eustatic and climatic controls on the development of the Wahiba Sand Sea, Sultanate of Oman. Sedimentology 51, 1359–1385.
Renforth, P., 2012. The potential of enhanced weathering in the UK. International Journal of Greenhouse Gas Control 10, 229–243.
Renforth, P., 2019. The negative emission potential of alkaline materials. Nature Communications 10 (article 1401, 8 pages).
Renforth, P., Henderson, G., 2017. Assessing ocean alkalinity for carbon sequestration. Rev. Geophys. 55. https://doi.org/10.1002/2016RG000533.
Renforth, P., Manning, D.A.C., Lopez-Capel, E., 2009. Carbonate precipitation in artificial soils as a sink for atmospheric carbon dioxide. Appl. Geochem. 24, 1757–1764.
Renforth, P., Washbourne, C.-L., Taylder, J., Manning, D.A.C., 2011. Silicate production and availability for mineral carbonation. Environ. Sci. Technol. 45, 2035–2041.
Renforth, P., Pogge von Strandmann, P.A.E., Henderson, G.M., 2015. The dissolution of olivine added to soil: implications for enhanced weathering. Appl. Geochem. 61, 109–118.
Rigopoulos, I., Delimitis, A., Ioannou, I., Efstathiou, A.M., Kyratsi, T., 2018a. Effect of ball milling on the carbon sequestration efficiency of serpentinized peridotites. Minerals Engineering 120, 66–74.
Rigopoulos, I., Harrison, A.L., Delimitis, A., Ioannou, I., Efstathiou, A.M., Kyratsi, T., Oelkers, E.H., 2018b. Carbon sequestration via enhanced weathering of peridotites and basalts in seawater. Applied Geochemistry 91, 197–207.
Rudge, J.F., Kelemen, P.B., Spiegelman, M., 2010. A simple model of reaction induced cracking applied to serpentinization and carbonation of peridotite. Earth Planet. Sci. Lett. 291, 215–227.
Rutqvist, J., 2015. Fractured rock stress-permeability relationships from in situ data and effects of temperature and chemical-mechanical couplings. Geofluids 15, 48–66.
Sadowski, A.J., Forson, C.K., Walters, M.A., Hartline, C.S., 2016. Compilation surface geologic map for use in three-dimensional structural model building at The Geysers geothermal field, northern California. In: Proc. 41st Workshop on Geothermal Reservoir Engineering, Stanford University, Stanford, California, February 22–24, 2016, SGP-TR-209.
Sanna, A., Uibu, M., Caramanna, G., Kuusik, R., Marato-Valer, M.M., 2014. A review of mineral carbonation technologies to sequester CO2. Chem. Soc. Rev. 43, 8049–8080.
Savaramini, A., Assima, G.P., Beaudoin, G., Larachi, F., 2014. Biomass torrefaction and CO2 capture using mining wastes–a new approach for reducing greenhouse gas emissions of co-firing plants. Fuel 115, 749–757.
Scarsi, M., Malatesta, C., Fornasaro, S., 2018. Lawsonite-bearing eclogite from a tectonic

mélange in the Ligurian Alps: new constraints for the subduction plate-interface evolution. Geol. Mag. 155, 280–297.
Schuiling, R.D., Krijgsman, P., 2006. Enhanced weathering: an effective and cheap tool to sequester CO2. Climatic Change 74, 349–354.
Seifritz, W., 1990. CO_2 disposal by means of silicates. Nature 345, 486.
Shevenell, L., 2012. The estimated costs as a function of depth of geothermal development wells drilled in Nevada. GRC Transactions 36, 121–128.
Sigfusson, B., Gislason, S.R., Matter, J.M., Stute, M., Gunnlaugsson, E., Gunnarsson, I., Aradottir, E.S., Sigurdardottir, H., Mesfin, K., Alfredsson, H.A., Wolff-Boensich, D., Arnarson, M.T., Oelkers, E.H., 2015. Solving the carbon dioxide buoyancy challenge: the design and field testing of a dissolved CO2 injection system. Int. J. Greenhouse Gas Control 37, 213–219.
Skarbek, R., Savage, H., Kelemen, P.B., 2018. Competition between crystallization-induced expansion and creep compaction during gypsum formation. J. Geophys. Res. 123, 5372–5393.
Snæbjörnsdóttir, S.Ó., Oelkers, E.H., Mesfin, K., Aradóttir, E.S., Dideriksen, K., Gunnarsson, I., Gunnlaugsson, E., Matter, J.M., Stute, M., Gislason, S.R., 2017. The chemistry and saturation states of subsurface fluids during the in situ mineralisation of CO2 and H2S at the CarbFix site in SW-Iceland. Int. J. Greenhouse Gas Control 58, 87–102.
Sofiya, A., Ishiwatari, A., Hirano, N., Tsujimori, T., 2017. Relict chromian spinels in Tulu Dimtu serpentinites and listvenite, Western Ethiopia: implications for the timing of listvenite formation. Int. Geol. Rev. 59, 1621–1631.
Stamboliadis, E., Pantelaki, O., Petrakis, E., 2009. Surface area production during grinding. Minerals Engineering 22, 587–592.
Stanger, G., 1985. Silicified serpentinite in the Semail nappe of Oman. Lithos 18, 13–22.
Streit, E., Kelemen, P., Eiler, J., 2012. Coexisting serpentine and quartz from carbonate-bearing serpentinized peridotite in the Samail Ophiolite, Oman. Contrib. Mineral. Petrol. 164, 821–837.
Styles, M.T., Elllison, R.A., Arkley, S.L.B., Crowley, Q.G., Farrant, A., Goudenough, K.M., McKervey, J.A., Pharaoh, T.C., Phillips, E.R., Schofield, D., Thomas, R.J., 2006. The Geology and Geophysics of the United Arab Emirates: Volume 2, Geology. UAE Ministry of Energy, Abu Dhabi, United Arab Emirates (351 pp.).
Taylor, L.L., Quirk, J., Thorley, R.M., Kharecha, P.A., Hansen, J., Ridgwell, A., Lomas, M.R., Banwart, S.A., Beerling, D.J., 2016. Enhanced weathering strategies for stabilizing climate and averting ocean acidification. Nature Climate Change 6, 402–408.
Taylor, L.L., Beerling, D.J., Quegan, S., Banwart, S.A., 2017. Simulating carbon capture by enhanced weathering with croplands: an overview of key processes highlighting areas of future model development. Biology Letters 13, 20160868.
Thom, J.G.M., Dipple, G.M., Power, I.M., Harrison, A.L., 2013. Chrysotile dissolution rates: implications for carbon sequestration. Appl. Geochem. 35, 244–254.
Tominaga, M., Beinlich, A., Lima, E.A., Tivey, M.A., Hampton, B.A., Weiss, B., Harigane, Y., 2017. Multi-scale magnetic mapping of serpentinite carbonation. Nature Communications 8. https://doi.org/10.1038/s41467-017-01610-4.
Tromans, D., 2008. Mineral comminution: energy efficiency considerations. Minerals Engineering 21, 613–620.
Ulrich, M., Munoz, M., Guillot, S., Cathelineau, M., Picard, C., Quesnel, B., Boulvais, P., Couteau, C., 2014. Dissolution–precipitation processes governing the carbonation and silicification of the serpentinite sole of the New Caledonia ophiolite. Contrib. Mineral. Petrol 167, 952. https://doi.org/10.1007/s00410-013-0952-8.
Ulven, O.I., Jamtveit, B., Malthe-Sorenssen, A., 2014a. Reaction driven fracturing of porous rocks. J. Geophys. Res. 119. https://doi.org/10.1002/2014JB011102.
Ulven, O.I., Storheim, H., Austrheim, H., Malthe-Sorenssen, A., 2014b. Fracture initiation during volume increasing reactions in rocks and applications for CO2 sequestration. Earth Planet Sci. Lett. 389, 132–142.
UNEP, 2018. The Emissions Gap Report 2018, United Nations Environment Program. https://www.unenvironment.org/resources/emissions-gapreport-2018.
US Energy Information Administration, 2018. U.S. Oil and Natural Gas Wells by Production Rate. https://www.eia.gov/petroleum/wells/.
US Energy Information Administration, 2020. Electric Power Monthly, Data for January 2020, Released March 24, 2020, Table 5.6.A. Average Price of Electricity to Ultimate Customers by End-use Sector.
US Environmental Protection Agency, 2017. Drinking Water Contaminants: Standards and Regulations. https://www.epa.gov/dwstandardsregulations.
Vanderzee, S.S.S., Dipple, G.M., Bradshaw, P.M.D., 2019. Targeting highly reactive labile magnesium in ultramafic tailings for greenhouse-gas offsets and potential tailings stabilization at the Baptiste deposit, central British Columbia (NTS 093K/13, 14). In: Geoscience BC Summary of Activities 2018: Minerals and Mining, Geoscience BC Report 2019-1, pp. 109–118.
Velbel, M.A., 2009. Dissolution of olivine during natural weathering. Geochim. Cosmochim. Acta 73, 6098–6113.
Vogt, C., Marquart, G., Kosack, C., Wolf, A., Clauser, C., 2012. Estimating the permeability distribution and its uncertainty at the EGS demonstration reservoir Soultz-sous-Forêts using the ensemble Kalman filter. Water Resour. Res. 48, W08517. https://doi.org/10.1029/2011WR011673.
Vogt, C., Klitzsch, N., Rath, V., 2014. On self-potential data for estimating permeability in enhanced geothermal systems. Geothermics 51, 201–213.
Wang, Y., Forssberg, E., Sachweh, J., 2004. Dry fine comminution in a stirred media mill—MaxxMill® Int. J. Mineral Processing 74, S65–S74.
Wikipedia, 2019. King Fahd International Airport. https://en.wikipedia.org/wiki/King_Fahd_International_Airport.
Wilcox, J., Psarras, P.C., Ligouri, S., 2017. Assessment of reasonable opportunities for direct air capture. Environ. Res. Lett. 12, 065001.
Wilcox, J., Psarras, P., Pilorgé, H., McQueen, N., Liguori, S., He, J., Yuan, M., Woodall, C., Kian, K., Pierpoint, L., Jurewicz, J., Lucas, J., Jacobson, R., Deich, N., 2020. Cost analysis of direct air capture and storage coupled to low-carbon energy resources in the U.S. Env. Sci. Tech (in review).
Wilde, A., Simpson, L., Hanna, S., 2002. Preliminary study of tertiary hydrothermal alteration and platinum deposition in the Oman ophiolite. J. Virtual Explorer 6, 7–13.
Wilson, S.A., Raudsepp, M., Dipple, G.M., 2006. Verifying and quantifying carbon fixation in minerals from serpentine-rich mine tailings using the Rietveld method with X-ray powder diffraction data. Am. Min. 91, 1331–1341.
Wilson, S.A., Dipple, G.M., Power, I.M., Thom, J.M., Anderson, R.G., Raudsepp, M., Gabities, J.E., Southam, G., 2009a. Carbon dioxide fixation within mine wastes of ultramafic-hosted ore deposits: examples from the Clinton Creek and Cassiar Chrysotile deposits, Canada. Econ. Geol. 104, 95–112.
Wilson, S.A., Raudsepp, M., Dipple, G.M., 2009b. Quantifying carbon fixation in trace minerals from processed kimberlite: a comparative study of quantitative methods using X-ray powder diffraction data with applications to the Diavik Diamond Mine, Northwest Territories, Canada. Appl. Geochem. 24, 2312–2331.
Wilson, S.A., Barker, S.L.L., Dipple, G.M., Atudorei, V., 2010. Isotopic disequilibrium during uptake of atmospheric CO2 into mine process waters: implications for CO2 sequestration. Environ. Sci. Technol. 44, 9522–9529.
Wilson, S.A., Dipple, G.M., Power, I.M., Barker, S.L.L., Fallon, S.J., Southam, G., 2011. Subarctic weathering of mineral wastes provides a sink for atmospheric CO2. Environ. Sci. Technol. 45, 7727–7736.
Wilson, S.A., Harrison, A.L., Dipple, G.M., Power, I.M., Barker, S.L.L., Mayer, K.U., Fallon, S.J., Raudsepp, M., Southam, G., 2014. Offsetting of CO2 emissions by air capture in mine tailings at the Mount Keith Nickel Mine, Western Australia: rates, controls and prospects for carbon neutral mining. Int. J. Greenhouse Gas Control 25, 121–140.
Wolery, T.J., 1979. Calculation of Chemical Equilibrium Between Aqueous Solution and Minerals: The EQ3/6 Software Package, UCRL-52658. Lawrence Livermore National Laboratory, Livermore, CA.
Wolery, T.J., 1992. EQ3/6, A Software Package for Geochemical Modeling of Aqueous Systems: Package Overview and Installation Guide (Version 7.0). Lawrence Livermore National Laboratory, Livermore, CA (66 pp.).
Zedef, V., Russell, M.J., Fallick, A.E., 2000. Genesis of vein stockwork and sedimentary magnesite and hydromagnesite deposits in the ultramafic terrains of southwestern Turkey: a stable isotope study. Econ. Geol. 95, 429–446.
Zeebe, R.E., Wolf-Gladrow, D., 2001. CO2 in seawater: equilibrium, kinetics, isotopes. In: Elsevier Oceanography Series No. 65. Elsevier, Amsterdam.
Zhang, Z., Jafarpour, B., Li, L., 2014. Inference of permeability heterogeneity from joint inversion of transient flow and temperature data. Water Resour. Res. 50, 4710–4725.
Zheng, X., Cordonnier, B., Zhu, W., Renard, F., Jamtveit, B., 2018. Effects of confinement on reaction-induced fracturing during hydration of periclase. G-cubed 19, 2661–2672.
Zheng, X., Cordonnier, B., McBeck, J., Boller, E., Jamtveit, B., Zhu, W., Renard, F., 2019. Mixed-mode strain localization generated by hydration reaction at crustal conditions. J. Geophys. Res. 124. https://doi.org/10.1029/2018JB017008.
Zhu, W., Fusseis, F., Lisabeth, H., Xing, T., Xiao, X., De Andrade, V., Karato, S.-I., 2016. Experimental evidence of reaction-induced fracturing during olivine carbonation. Geophys. Res. Lett. 43, 9535–9543.